

Department of Precision and Microsystems Engineering

Multi-resolution space-time topology optimization

Budhaditya Chakraborty

Report no : 2023.071
Coach : Ir. Kai Wu
Professor : Dr. Jun Wu, Dr. Ir. A. van Keulen
Specialisation : Computational Design and Mechanics(CDM)
Type of report : M.Sc. Thesis
Date : 20 September 2023



Multi-resolution space-time topology optimization

by

Budhaditya Chakraborty

to obtain the degree of Master of Science

at the Delft University of Technology,

to be defended publicly on Wednesday September 20, 2023 at 10:00 AM.

Student number: 5479398
Project duration: September 1, 2022 – September 20, 2023
Thesis committee: Prof. dr. J. Wu, TU Delft(IDE-SDE), supervisor
Prof. dr. C. Ayas, TU Delft(3mE-PME)
Ir. K. Wu, TU Delft(3mE-PME)

An electronic version of this thesis is available at <http://repository.tudelft.nl/>.

Summary

In the realm of traditional additive manufacturing, design and fabrication sequence planning have historically followed separate tracks. However, recent strides in the field, particularly in the utilization of robotic arms with multiple degrees of freedom, have brought forth a revolutionary approach known as Space-Time Topology Optimization (STTO). This groundbreaking algorithm breaks down the barriers between design and fabrication by simultaneously optimizing the structure and fabrication sequence. It achieves this feat by employing density and time fields as design variables, allowing for a holistic and integrated approach to the manufacturing process. However, within the framework of STTO, multiple iterations of finite element computations become necessary. This results in a substantial computational burden throughout the overall process.

My contribution within STTO lies in its adoption of a multi-resolution strategy. This strategy enables the use of different resolutions for the design fields, enhancing computational efficiency. Coarsening, a critical component of this strategy, is implemented through a sophisticated weighted average scheme. This coarsening process facilitates the construction of stiffness matrices with significantly reduced finite element calculations, resulting in substantial time savings during the optimization process.

The impact of coarsening in STTO has been rigorously studied across various levels, yielding remarkable results and advantages. In 2D scenarios, this approach has achieved an impressive 5-fold reduction in computation time, while in the more complex 3D domain, it has led to an astounding 30-fold decrease. Moreover, it's worth noting that compliance, a crucial performance metric, maintains its integrity even with coarsening, with compliance drop remaining below 5% for levels deemed acceptable. This study illuminates the profound implications of coarsening within the STTO framework, emphasizing the significant strides made in computational efficiency while ensuring structural integrity and performance.

Contents

Summary	i
1 Introduction	1
1.1 Topology optimization with additive manufacturing	2
1.2 Space-time topology optimization	3
1.3 Computational complexity of topology optimization and space-time topology optimization	4
1.4 Multi-resolution approach to space-time topology optimization	6
1.5 Thesis structure	6
2 Literature review	8
2.1 Density based topology optimization	8
2.1.1 SIMP and modified SIMP methods	8
2.1.2 Filtering techniques	9
2.1.3 Objective function and constraint function	10
2.1.4 Sensitivity analysis	10
2.1.5 Optimizer - optimality criteria and method of moving asymptotes	10
2.2 Space-time topology optimization	11
2.2.1 The objective function	11
2.2.2 Generating intermediate structures	11
2.2.3 Volume and continuity constraint on intermediate structures	13
2.2.4 Space-time problem formulation	13
2.3 Computational complexity of topology optimization	14
2.4 Comparison of various coarsening methods	14
2.4.1 Higher-order multi-resolution topology optimization using finite cell method	14
2.4.2 Design and analysis adaptivity in multi-resolution topology optimization	16
2.4.3 Multi-resolution topology optimization (MTOPT)	17
2.4.4 Coarsening in multigrid methods	18
2.4.5 Comparison of coarsening strategies	19
3 Multi-resolution scheme	21
3.1 Weighted average coarsening	21
3.1.1 Creating one coarse element	21
3.1.2 Creating the restriction operator for an assembled fine mesh stiffness matrix	21
3.1.3 Comparison of the approaches	23
3.2 Sizing factor for coarsening of element	24
3.3 Validation strategies for the coarsening method	25
3.4 Using the interpolation operator	26
3.5 Extension of the coarsening operator along the lines of multigrid	27
3.5.1 Higher degree coarsening: from 2x2 to 4x4 to 8x8	27
3.5.2 Incorporating higher degree coarsening in the standard topology optimization workflow	28
3.6 Extension to 3D	29
3.7 Topology optimization formulation	30
3.7.1 Application of operator to topology optimization	30
3.7.2 Final formulation for topology optimization	31
3.7.3 Sensitivity analysis for topology optimization	31
3.8 Space-time problem formulation	31
3.8.1 Application of operator to space-time topology optimization	31
3.8.2 Final formulation for space-time topology optimization	32
3.8.3 Sensitivity analysis for space-time topology optimization	32

4	Results and discussion	34
4.1	Topology optimization results with coarsening operator	34
4.2	Space-time topology optimization results	36
4.3	3D topology optimization results	38
4.4	Comparison with the trimesh method coarsening strategy	41
5	Conclusion and future scope	44
5.1	Conclusion	44
5.2	Future scope	44
	References	46

1

Introduction

The concept of topology optimization as introduced by Bendsøe and Kikuchi [7] emerged as a pioneering mathematical technique aimed at redistributing material within a given design domain to achieve optimal structural performance. This innovative approach sought to answer the question of how material should be allocated to achieve specific engineering objectives while adhering to constraints. This marked the inception of a powerful optimization method that continues to evolve and find applications across various industries today.

In its early stages, topology optimization primarily emphasized achieving structural performance while minimizing material usage and creating smoother, more continuous shapes for components. However, as additive manufacturing and the interest in discrete lattice structures gained prominence, topology optimization research began to shift towards investigating both continuum and discrete structures. This evolution allows designers and engineers to leverage a wider range of tools to optimize components and products, aligning with advancements in manufacturing technologies.

The emergence of the Optimality Criteria (OC) method introduced by Bendsøe[8] marked a significant milestone in topology optimization. The Optimality Criteria (OC) method introduced a computational framework aimed at expediting convergence towards an optimal condition by iteratively adjusting the design variables based on certain optimality criteria. This advancement not only accelerated the exploration of design alternatives but also paved the way for more complex and realistic optimization problems to be tackled effectively.

Topology optimization has gained substantial traction within engineering and design communities. This surge in popularity was fueled by advancements in computer hardware and optimization algorithms, which significantly enhanced the capability to address intricate geometries and intricate design challenges. These developments led to broader application across various industries, including aerospace, automotive, and biomedical fields. The newfound ability to handle complex geometries and incorporate intricate constraints fostered innovative design solutions that were both structurally efficient and manufacturable. As a result, topology optimization became a pivotal tool for engineers and designers aiming to push the boundaries of traditional design paradigms.

The growing interest in additive manufacturing aligns seamlessly with the principles of topology optimization. The advent of additive manufacturing has revolutionized traditional manufacturing methods by enabling the creation of intricate and complex structures that were previously challenging to manufacture using conventional techniques. This technological synergy aligns well with the core tenets of topology optimization, which seeks to find the most efficient and optimal distribution of material within a given design space. As additive manufacturing techniques evolve and become more sophisticated, the partnership between topology optimization and additive manufacturing is further strengthened, paving the way for groundbreaking advancements in design and manufacturing.

In conclusion, topology optimization has emerged as a groundbreaking mathematical technique, initially focused on reshaping material within design domains to achieve optimal structural performance. Early

research primarily concentrated on continuum structures, but as technology evolved, it encompassed discrete structures as well. Over time, topology optimization gained widespread traction in engineering and design communities, thanks to advancements in hardware and optimization algorithms. These developments empowered engineers and designers to tackle intricate geometries and constraints across various industries. Moreover, the synergy between topology optimization and additive manufacturing is driving innovation, promising remarkable advancements in design and manufacturing.

1.1. Topology optimization with additive manufacturing

The fusion of topology optimization and additive manufacturing marks a significant milestone in the realm of generative design. This synergy leverages the capabilities of both fields to achieve a new level of design freedom, efficiency, and sustainability. By integrating topology optimization's ability to optimize material distribution with additive manufacturing's precision in fabricating complex geometries, industries can now create optimized structures that are not only lightweight but also tailored to specific performance requirements. This transformative approach has the potential to reshape various industries, offering innovative solutions that were previously unattainable using traditional design and manufacturing methodologies.

Topology optimization and additive manufacturing (AM) form a synergistic partnership rooted in their shared capabilities. AM's unique ability to construct intricate and complex geometries layer by layer complements topology optimization's strength in generating intricate material distributions. This harmony enables the creation of designs that were previously unfeasible using conventional manufacturing methods. AM's potential to fabricate complex lattice structures aligns perfectly with topology optimization's purpose. By determining the optimal arrangement of struts and voids in these lattices, topology optimization ensures lightweight yet robust components that leverage the full potential of AM techniques. Furthermore, AM's capability to produce parts with anisotropic material properties aligns with topology optimization's capacity to account for these anisotropic qualities, leading to tailored designs that harness the material's strengths in specific directions.

In addition to these synergies, the marriage of topology optimization and AM offers a range of practical benefits. Rapid prototyping becomes a reality, allowing for swift iteration and testing of new designs. Furthermore, AM's potential to fabricate intricate components as single units reduces the need for complex assembly, streamlining the manufacturing process. This powerful combination also fosters design exploration, facilitating the exploration of novel concepts and pushing the boundaries of what's achievable in both design and manufacturing.



Figure 1.1: Fused Deposition Modeling [20]

Wire Arc Additive Manufacturing (WAAM) and Fused Deposition Modeling (FDM) are two prominent additive manufacturing techniques that have revolutionized the manufacturing landscape. WAAM utilizes electric arcs to melt metal wire to fabricate large-scale metal parts layer by layer. This technique is lauded for its ability to swiftly produce complex, high-strength components, making it particularly well-suited for industrial applications. On the other hand, FDM operates by extruding thermoplastic materials layer by layer to construct objects. FDM's simplicity, versatility, and accessibility make it a popular choice for rapid prototyping and small-scale production. Both WAAM and FDM highlight the potential of additive manufacturing to create intricate geometries and optimize material utilization, ushering in a new era of manufacturing possibilities.

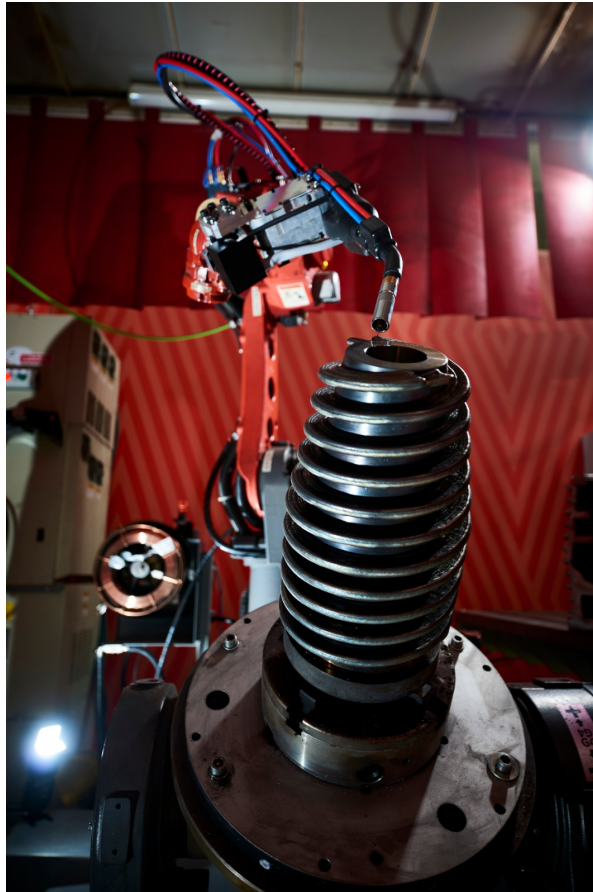


Figure 1.2: Wire arc additive manufacturing [25]

Additive Manufacturing (AM) processes are profoundly influenced by the sequence in which material is deposited, as it directly impacts factors like overhangs, support structures, and thermal stress accumulation. In this context, topology optimization can be further developed as a valuable tool [32], seamlessly integrating manufacturing order planning with design considerations. By optimizing both the structural layout and the sequence of material addition, topology optimization ensures not only functional designs but also efficient fabrication processes. Additionally, AM frequently relies on support structures to address overhangs during printing. Topology optimization, with its ability to create intricate and self-supporting geometries, can significantly diminish the need for such supports, streamlining the manufacturing process and enhancing the feasibility of additive manufacturing techniques as per Langelaar[22].

1.2. Space-time topology optimization

In traditional design processes, there exists a clear separation between structural design and manufacturing order planning. This conventional approach treats these two stages as distinct and separate steps, often resulting in challenges. One significant challenge is that this separation can lead to subopti-

mal designs. This is because the design phase may not adequately consider manufacturing constraints, such as material deposition sequence, overhangs, and support requirements. As a result, designs optimized solely based on structural criteria might encounter difficulties during the manufacturing phase, leading to increased costs, time, and potential design modifications. This lack of synchronization between design and manufacturing stages hinders the ability to achieve holistic and efficient solutions.

Space-time topology optimization introduced by Wang et al. [32] represents a transformative approach that addresses the separation between structural design and manufacturing order planning. This method introduces a unified optimization process where the structural design and the manufacturing order are integrated seamlessly. At its core, space-time topology optimization employs two distinct design fields: the density field for material distribution and the time field for determining the sequence of material addition during fabrication. This dual-field approach enables the optimization of both design and manufacturing considerations in a single coherent framework. By optimizing these variables concurrently, the approach ensures that the resulting designs are not only structurally efficient but also compatible with the additive manufacturing process.

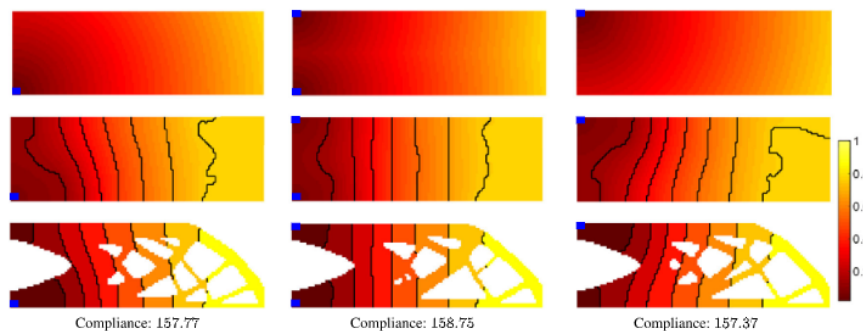


Figure 1.3: The images depict various time fields and the corresponding structures produced using different manufacturing starting points, represented by the blue regions. From top to bottom, we observe the initial time fields, which are constructed based on distance fields related to the starting points, followed by the optimized time fields and the resulting optimized structures. The black curves demarcate boundaries between parts manufactured in distinct manufacturing stages. Notably, the number of stages, set at 8 in this particular test, remains constant and is not a design variable; hence, the values denoted as T_i that segment the time field are predefined. The colorbar on the right provides a reference for the time values.[32]

One of the key advantages of space-time topology optimization lies in its ability to integrate manufacturing constraints directly into the optimization process. This integration means that challenges such as overhangs, support requirements, and thermal stress accumulation can be addressed during the design phase itself. This eliminates the need for subsequent modifications or adjustments to the design after it has been optimized, streamlining the overall design-to-manufacturing process. The space-time topology optimization approach thus marks a significant departure from traditional methodologies by offering a holistic solution that harmonizes structural design and manufacturing order planning.

1.3. Computational complexity of topology optimization and space-time topology optimization

Traditional topology optimization involves several computationally demanding steps. The computational complexity is typically denoted using the big O notation, explained by Chivers[12]. For instance, it is expressed as $O(n)$ in many cases. Here O represents the order of, or big O, indicating the upper bound or worst case scenario of the algorithm. n represents the number of inputs, here the number of degrees of freedom to be solved for.

The most computationally intensive aspect is the finite element analysis step. Solving equations i.e. the equation $u = F/K$ where K is the stiffness matrix, F is the force vector and u is the displacement vector for each finite element, this operation entails dense linear algebra, leading to a complexity of $O(n^3)$, described by Aage[1]. Additionally, sensitivity analysis, which relies on the solution of the finite element analysis, shares a complexity similar to FEM analysis, contributing to the computational load. Consequently, the complexity of this analysis step governs the overall computational requirements of traditional topology optimization. Furthermore, the optimization algorithm's choice, often relying on

gradient-based methods, may extend computational demands due to the potential need for numerous iterations.

The complexity of the objective function varies significantly between traditional and space-time topology optimization. In traditional methods, the objective function is primarily concerned with the compliance of the overall structure, reflecting its load-bearing capability. However, in space-time topology optimization, the objective function encompasses compliance evaluations for both the complete structure and each intermediate stage of fabrication. This inclusion of manufacturing order planning introduces a multifaceted evaluation, allowing the space-time approach to optimize design and manufacturability simultaneously.

	Assembly	Solving FEM Equation	Density Update(using OC)
Topology Optimization	8.3	21.6	3.8

(a) Computation times for topology Optimization

Compliance of Entire structure		Compliance of intermediate			
Assembly	Solving FEM	Assembly per stage	For 8 stages	Solving FEM per stage	For 8 stages
8.5	20.3	8.8	70.4	22.1	176.8

(b) Computation times per iteration for space-time topology optimization

	Assembly Total	Solving FEM equation Total	Density Update (using MMA)
Space-time topology optimization	78.9	197.1	174.4

(c) Computation times per iteration for entire structure and intermediate structures

Table 1.1: Comparison of computational complexity for standard topology optimization and space-time topology optimization. A mesh of 120×40 elements was used for both. 8 stages were chosen for space-time topology optimization. (All times are in milliseconds)

Space-time topology optimization introduces a stage-wise computation approach, dividing the fabrication process of a structure into multiple intermediate stages. As the number of stages increases, the computational complexity of the optimization process escalates accordingly. Each iteration requires calculating the compliance not only for the final structure but also for each individual stage in the manufacturing sequence. This multiplies the intricacy of compliance calculations, resulting in a notable increase in the overall computational burden of the space-time optimization process.

In Tables 1.1a, 1.1b, and 1.1c, we've recorded computation times within the optimization workflow. Table 1.1a specifically focuses on standard topology optimization, highlighting key components like stiffness matrix assembly, solving the linear FEM equation ($u = F/K$ where K denotes the stiffness matrix, F is the force vector, and u is the displacement vector for each finite element), and the time needed for the optimizer to update density variables.

Table 1.1b maintains a similar structure but offers a more detailed breakdown. It dissects computation times into evaluating the compliance for the entire structure and intermediate structures. These evaluations are further divided into time spent on assembling the stiffness matrix and solving the linear equation. In this test, we adopted 8 stages, necessitating the calculation of compliance for each of these stages per iteration.

Table 1.1c consolidates the results from Table 1.1b, encompassing assembly, linear equation solving, and density variable updates. Notably, due to the multiple compliance calculations across various stages, space-time optimization experiences nearly a tenfold increase in per-iteration computation compared to standard topology optimization.

Efficiently addressing the heightened computational complexity brought about by space-time optimization demands algorithmic enhancements that can navigate the intricacies of optimizing intermediate stages while maintaining computational efficiency. To manage the increased load of compliance calculations across multiple stages, the integration of intelligent algorithms and strategic computational shortcuts becomes crucial. These algorithmic innovations aim to strike a balance between accuracy and computational feasibility within the space-time optimization framework.

1.4. Multi-resolution approach to space-time topology optimization

Space-time topology optimization has proven to be a powerful tool for obtaining efficient and manufacturable designs that evolve over time. However, the computational demands associated with solving the finite element method (FEM) equation in each iteration can become substantial, especially for large and complex optimization problems. To address this challenge, a multi-resolution approach can be adopted, offering significant computational advantages while maintaining design quality.

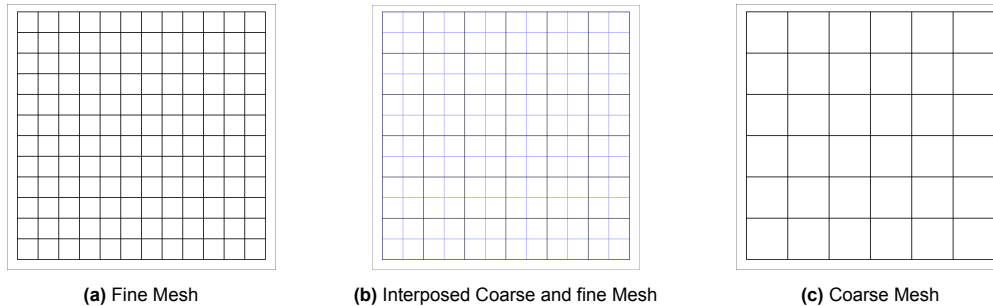


Figure 1.4: Representation of intended multi-resolution approach by using a fine mesh and a coarse mesh

The core idea of the multi-resolution approach is to generate coarser versions of the stiffness matrices obtained from the fine mesh densities. Instead of solving the FEM equation on the fine mesh, the optimization process focuses on coarser meshes, reducing the number of degrees of freedom and thus decreasing the computation time. The coarser versions of the stiffness matrices capture the essential characteristics of the problem while avoiding unnecessary fine-scale details that might not significantly affect the overall performance of the structure.

Figure 1.4 provides an overview of the intended approach. Here, densities are defined on the fine mesh, but the goal is to create a representation of the stiffness matrix on a coarse mesh. This coarse mesh will have fewer degrees of freedom, reducing the computational load during linear equation solving. Each coarse element in Figure 1.4b contains a variable number of fine mesh elements (e.g., four in this illustration, but this can vary). The transfer of information between these fine and coarse mesh elements is crucial. Accurate information transfer ensures that fine-scale features from the fine mesh are appropriately represented in the stiffness matrix of the coarse mesh.

By coarsening the stiffness matrices, the optimization process can efficiently handle large-scale designs without compromising the final design quality. The coarser meshes enable the optimizer to obtain solutions that are more tractable while containing the increase in compliance of the structure within a predefined threshold. This approach strikes a balance between computational efficiency and design accuracy, making it an attractive choice for complex space-time topology optimization problems.

Implementing the multi-resolution approach requires careful consideration of the coarsening technique, interpolation methods, and their integration into the optimization workflow. The coarser versions of the stiffness matrices are transferred back to the fine mesh through interpolation, allowing the optimizer to iteratively refine the design while maintaining overall computational efficiency.

In summary, the multi-resolution approach in space-time topology optimization offers a practical solution to reduce computational demands without sacrificing design quality. By generating coarser versions of the stiffness matrices and focusing on the essential regions of the design, the optimizer can efficiently explore the design space while containing the increase in compliance within a controlled threshold. This approach enables the solver to handle larger and more complex optimization problems, making space-time topology optimization a more versatile tool for designing efficient and manufacturable structures.

1.5. Thesis structure

The thesis structure comprises three primary chapters, each building upon the previous to culminate in a comprehensive exploration of topology optimization. In Chapter 2, a detailed examination of the fundamental components of topology optimization is conducted. This chapter delves into the intricacies of space-time topology optimization and rigorously assesses the computational complexities inherent

to each step of this advanced process. Within this context, the chapter identifies a critical gap in the optimization process, the need for an effective coarsening strategy. It proceeds to explore several coarsening strategies commonly found in the existing body of literature.

Chapter 3 shifts the focus to the practical implementation of the identified coarsening strategy. This includes the extension of the coarsening technique to higher-order coarsening levels and, subsequently, the three-dimensional domain. The chapter serves as a bridge between theoretical understanding and practical application, offering valuable insights into the complexities of bringing such strategies to life.

In Chapter 4, the thesis presents the results obtained from the implemented coarsening strategy. These results are analyzed and compared with a rival coarsening strategy to discern the advantages and limitations. Finally, Chapter 5 consolidates the findings and lessons learned throughout the thesis, drawing meaningful conclusions.

2

Literature review

Topology optimization comprises a range of techniques aimed at achieving optimal material distribution within a design space to meet specific structural performance criteria and constraints. These methods vary in their mathematical formulations, optimization strategies, and handling of design variables. For example, the Solid Isotropic Material with Penalization (SIMP), introduced by Bendsøe and Kikuchi [9], approach directly manipulates material densities, while others focus on altering geometric boundaries or effective material properties. These methods offer unique benefits and complexities, catering to different problem complexities, goals, and computational capacities. This diverse array of methodologies enriches the field of topology optimization, providing a toolkit to tackle various engineering and design challenges effectively.

2.1. Density based topology optimization

Density based topology optimization is a widely used approach in engineering design to determine the optimal distribution of material within a given design domain. This section will delve into the key components of density based topology optimization, including the SIMP (Solid Isotropic Material with Penalization) and modified SIMP methods, the density filter, the objective and constraint functions, and the optimization model. Additionally, the importance of sensitivity analysis is explored and a comparison is drawn into the use of the Optimality criteria (OC) optimizer and the Method of moving asymptotes (MMA) optimizer for this problem.

2.1.1. SIMP and modified SIMP methods

The SIMP method, introduced by Bendsøe and Kikuchi [9], is a fundamental density based topology optimization approach. It employs a penalization scheme to continuously interpolate between void (completely empty) and solid material regions. The density variable in each element represents the material volume fraction, and a high penalization factor penalizes intermediate densities, encouraging binary material distribution. For every element e , with a density value of x , a penalization factor p is used to ascertain the stiffness of the element E_e .

$$E_e(x_e) = x_e^p \quad (2.1)$$

The modified SIMP approach, as introduced by Bendsøe [7] and then Zhou et al. [34] uses E_0 and E_{min} wherein E_0 stands for the stiffness of the material being used and E_{min} is a very small value used to avoid the stiffness matrix becoming singular. The modified SIMP approach stands as:

$$E_e(x_e) = E_{min} + x_e^p(E_0 - E_{min}) \quad (2.2)$$

While the SIMP method has been highly successful in producing optimal designs, it can suffer from numerical instabilities wherein the stiffness matrix may become singular and the so-called "checkerboard" pattern problem.

To mitigate the checkerboard pattern issue, some modified SIMP methods have been introduced. These methods introduce additional filtering or regularization techniques to smooth the density distribution, leading to improved convergence and stability. The introduction of density filters, which will be discussed next, is one such regularization approach that promotes the formulation of continuous material regions, helping to alleviate the checkerboard problem.

2.1.2. Filtering techniques

The need for filtering techniques in topology optimization arises from the inherent challenge of dealing with discrete design variables within a continuous design space. In this optimization process, material distribution is represented by a discrete set of design variables, such as density values assigned to finite elements. These discrete variables can result in designs with sharp and unrealistic transitions between materials, making them challenging to manufacture and analyze. Filtering techniques address this issue by smoothing and regularizing the material distribution, promoting more manufacturable and physically plausible designs while maintaining optimization efficiency. They play a crucial role in achieving the balance between design feasibility and structural performance, making topology optimization a practical tool for engineering and design applications.

Density filters are crucial components in density-based topology optimization, particularly for mitigating the checkerboard pattern and improving structural representation. Filters, such as the density based filter smooth the material distribution by averaging the densities of neighboring elements. By applying these filters, the density variables are averaged, ensuring that the optimized designs exhibit continuous material regions, which can be more readily interpreted for manufacturing purposes as explained by Diaz [14], Jog et al.[21], Sigmund[28]. The choice of the filter and its parameters significantly influences the outcome of the optimization process, and appropriate filter settings based on the problem requirements.

The sensitivity filter introduced by Sigmund et al.[27] modifies the sensitivities $\partial c/\partial x_e$ as:

$$\frac{\partial c}{\partial x_e} = \frac{1}{\max(\gamma, x_e) \sum_{i \in N_e} H_{ei}} \sum_{i \in N_e} H_{ei} x_i \frac{\partial c}{\partial x_i} \quad (2.3)$$

where c is the compliance function being evaluated, N_e is the set of elements i for which the center-to-center distance $\Delta(e, i)$ to element e is smaller than the filter radius r_{min} and H_{ei} is a weight factor defined as

$$H_{ei} = \max(0, r_{min} - \Delta(e, i)) \quad (2.4)$$

The term $\gamma = 10^{-3}$ is a small positive number to avoid division by zero.

The density filter modifies the densities as:

$$\tilde{x}_e = \frac{1}{\sum_{i \in N_e} H_{ei}} \sum_{i \in N_e} H_{ei} x_i \quad (2.5)$$

For a filter with radius r_{min} and taking $\Delta(e, i)$ as the centre to centre distance between the centre element e and another element i , within the filter, the filter is defined as:

$$H_{ei} = \max(0, r_{min} - \Delta(e, i)) \quad (2.6)$$

Density and sensitivity filters are distinct tools used in the context of topology optimization. The density filter is applied directly to the material density field, smoothing abrupt changes in material distribution to yield more manufacturable and continuous structures. In contrast, the sensitivity filter is used during sensitivity analysis, influencing the gradients computed for the optimization algorithm without directly affecting material distribution. While the density filter aims to improve convergence by providing a well-behaved material layout, the sensitivity filter assists in optimization convergence by offering precise gradients, particularly in areas with discontinuities in the objective function. These filters serve complementary roles in the topology optimization process.

2.1.3. Objective function and constraint function

The objective function in density based topology optimization quantifies the performance measure to be maximised or minimised. Commonly objective functions are for maximising structural stiffness or for minimising compliance, weight or displacement. The constraint function, on the other hand, enforces certain design requirements such as volume constraints, stress constraints or manufacturing constraints. Balancing the objective and constraint functions is crucial for obtaining designs that meet both performance targets and design constraints effectively.

For a compliance minimization problem, the general objective function and constraints are:

$$\min : c(x) = U^T K U = \sum_{e=1}^N E_e(x_e) u_e^T k_0 u_e \quad (2.7)$$

subject to:

$$\begin{aligned} V(x)/V_0 &= f \\ K U &= F \\ 0 &\leq x \leq 1 \end{aligned} \quad (2.8)$$

In these equations, c is the compliance, U and F are the global displacement and force vectors, respectively, K is the global stiffness matrix, u_e is the element displacement vector, k_0 is the element stiffness matrix for an element with unit Young's modulus, x is the vector of design variables (i.e. element densities), N is the number of elements used to discretize the design domain, $V(x)$ and V_0 are the material volume and design domain volume, and f is the prescribed volume fraction.

2.1.4. Sensitivity analysis

Sensitivity analysis is a critical aspect of density based topology optimization as it provides the gradients necessary for updating the density variables in each iteration. These gradients indicate how changes in the density variables impact the objective and constraint functions. Accurate sensitivity analysis ensures efficient convergence of the optimization process and helps achieve optimal designs. The sensitivity analysis for the objective function defined in equation 2.7 with respect to the density field can be derived as:

$$\frac{\partial c}{\partial x_e} = -p x_e^{p-1} (E_0 - E_{min}) u_e^T k_0 u_e \quad (2.9)$$

$$\frac{\partial V}{\partial x_e} = 1 \quad (2.10)$$

2.1.5. Optimizer - optimality criteria and method of moving asymptotes

The optimality criteria (OC) optimizer and the method of moving asymptotes (MMA) optimizer are two commonly used algorithms for solving density based topology optimization problems. The optimality criteria optimizer employs a heuristic approach adjusting the design variables iteratively to meet the specified constraints and objectives. While it is straightforward to implement, it may require tuning of parameters to achieve optimal convergence.

On the other hand, the MMA optimizer is a more sophisticated mathematical optimization technique. It provides a rigorous solution to the optimization problem by iteratively updating the design variables based on the gradients of the objective and constraint functions. MMA typically demonstrates faster convergence and improved robustness compared to the optimality criteria optimizer but may require more computational resources.

In conclusion, density based topology optimization is a powerful approach for determining optimal material distributions in engineering design. The SIMP and modified SIMP methods, density filters, objective and constraint functions, and sensitivity analysis are critical components in this process. Choosing appropriate algorithms such as the optimality criteria optimizer or MMA optimizer, depends on the problem complexity and computational resources available. Careful consideration of these components is essential for achieving accurate and efficient density based topology optimization results.

2.2. Space-time topology optimization

Space-time topology optimization represents an innovative paradigm that bridges the longstanding gap between material distribution in a design space and the intricacies of manufacturing order planning. Traditionally, these two essential aspects have been treated as distinct processes, often leading to suboptimal designs or complicated post-optimization adjustments. However, the emergence of space-time optimization introduces a transformative approach by seamlessly integrating both considerations through the introduction of two distinct design fields. The first field, the density field, serves as a representation of material distribution within the design, offering a unique perspective on structural layout. Simultaneously, the second field, the time field, takes on the role of a manufacturing order plan, delineating the sequence of construction for different parts of the design.

This integration of material distribution and manufacturing order within a unified framework holds immense potential for enhancing the efficiency and effectiveness of the design process. With the incorporation of the time field, the concept of intermediate structures comes into play, allowing for the creation of sectional geometries that will be printed at different time points. This temporal dimension not only adds a new layer of complexity to topology optimization but also provides a means to address manufacturing-related challenges in a holistic manner. As a result, space-time topology optimization heralds a new era where design and manufacturing intricacies are harmoniously orchestrated, enabling the realization of more efficient, functional, and manufacturable structures.

2.2.1. The objective function

The section delves into the objective function of space-time topology optimization, which is composed of dual components. The initial segment encapsulates the overall material property, for example compliance, inherent to the entire structure. In parallel, the subsequent component reflects the material property pertaining to the intermediate structures, further enriching the optimization process.

$$J(\rho, t) = J_{complete}(\rho, t) + J_{process}(\rho, t) \quad (2.11)$$

wherein,

$$J_{complete} = U^T K(\rho) U \quad (2.12)$$

$$J_{process} = \sum_{i=1}^N \alpha_i (U^{T_i})^T K(\rho^{T_i}) (U^{T_i}) \quad (2.13)$$

here U is the displacement vector, K is the assembled stiffness matrix and α is the weighting factor for the intermediate structures.

2.2.2. Generating intermediate structures

Utilizing finite element discretization within the design space, each element is assigned a (pseudo) density value $\rho_e \in [0, 1]$ and a (pseudo) time value $t_e \in [0, 1]$. The density value signifies whether the element is either empty ($\rho_e = 0$) or solid ($\rho_e = 1$) within the final structure. Simultaneously, the time value denotes the sequential addition of material to the element within the structure. Larger time values correspond to later fabrication instances. Similar to conventional density-based methodologies, the density value ultimately converges to either 0 or 1.

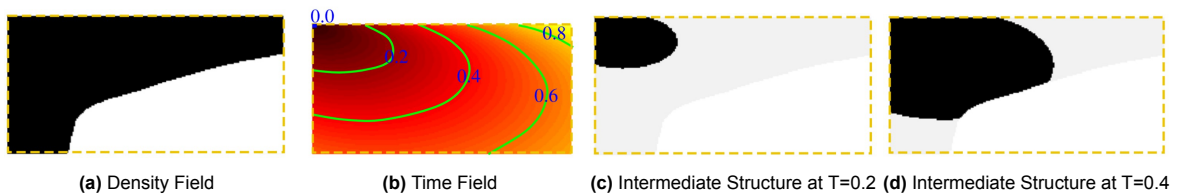


Figure 2.1: Illustration of a discrete density field (a), a continuous time field (b), and resulting intermediate structures at $T=0.2$ (c) and $T=0.4$ (d)[32].

In the presented space-time topology optimization, elements with time values $t_e \leq T$ contribute to the structure at a given time T . This has been illustrated in figure 2.1. Consequently, the intermediate

structure at time T is defined by

$$\rho_e^{[T]} = \begin{cases} \rho_e, & \text{if } t_e \leq T \\ 0, & \text{otherwise} \end{cases} \quad (2.14)$$

The projection method has been discussed by Wang et al. [30]. To avoid the use of piecewise functions which are conditional and hence not differentiable, a filtering technique is used to generate the intermediate structures from the density and time field. The design variables ϕ and τ are used for density and time design variables. To avoid checkerboard patterns, convolution operators are applied to smooth both fields. This results in $\tilde{\phi}$ and $\tilde{\tau}$ for the density field and time field respectively.

$$\tilde{\phi} = \frac{\sum_{i \in S_e} w(x_i, r_d) v_i \phi_i}{\sum_{i \in S_e} w(x_i, r_d) v_i} \quad (2.15)$$

and

$$t_e = \tilde{\tau} = \frac{\sum_{i \in S_e} w(x_i, r_d) v_i \tau_i}{\sum_{i \in S_e} w(x_i, r_d) v_i} \quad (2.16)$$

where v_i is the area or the volume of the element and the weighting function is defined as,

$$w(x_i, r) = r - \|x_i - x_e\| \quad (2.17)$$

where r is the filter radius, x_e and x_i are the positions of the centroid of the element e and neighbouring element $i \in S_e = \{i | w(x_i, r) > 0\}$. Also, the filter radius r_t for time and r_d for density can take different values. r_d also helps to control the thickness of the resulting structures.

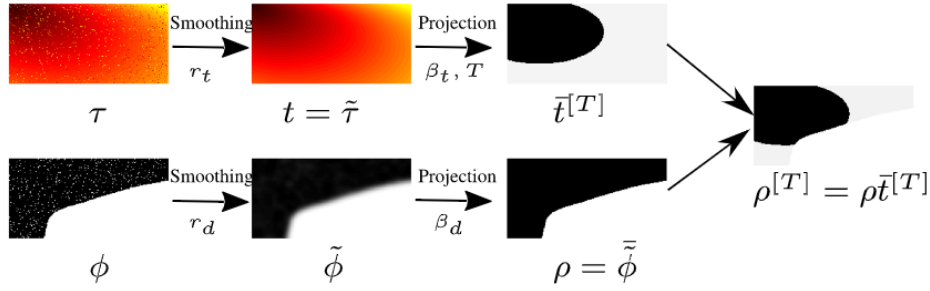


Figure 2.2: Image showing the density field (bottom), the time field (top) and the corresponding filtering and projection operators for generating an intermediate structure (right)[32]

After the smoothing operator, a smoothed Heaviside projection is applied to generate discrete values $\rho = \tilde{\phi}$ and \bar{t} , with the bar indicating the projected time fields. The projection is applied by,

$$\rho_e = \tilde{\phi}_e = \frac{\tanh(\beta_d \eta) + \tanh(\beta_d (\tilde{\phi}_e - \eta))}{\tanh(\beta_d \eta) + \tanh(\beta_d (1 - \eta))} \quad (2.18)$$

where β_d is a positive number to control the sharpness of the shape function, and $\eta = 0.5$ is the density threshold value.

For the time field, a projection is used to convert a time value smaller or larger than a given threshold T in time, to close to 1 or 0 respectively. This is done by:

$$\tau_e^{[T]} = 1 - \frac{\tanh(\beta_t T) + \tanh(\beta_t (t_e - T))}{\tanh(\beta_t T) + \tanh(\beta_t (1 - T))} \quad (2.19)$$

where β_t , similar to β_d controls the projection sharpness, and T is the threshold time value.

The intermediate structure at time T is defined by

$$\rho_e^{[T]} = \rho_e t_e^{[T]} \quad (2.20)$$

The process has been explained with the help of an illustration in figure 2.2.

2.2.3. Volume and continuity constraint on intermediate structures

The fabrication speed, representing material deposition per unit time, is a key factor in this process. To integrate it into space-time optimization, the time range $[0, 1]$ is discretized into $N + 1$ uniformly distributed timepoints, which is

$$T_i = \frac{i}{N}, \quad i = 0, \dots, N \quad (2.21)$$

here N is the number of stages each with a duration of $\frac{1}{N}$. Taking a constant fabrication speed, the increment in volume in each time interval is then $\frac{V_0}{N}$, hence

$$V^{[T_i]} \leq \frac{i}{N} V_0, \quad i = 1, \dots, N, \quad (2.22)$$

Here $V^{[T_i]}$ is given by

$$V^{[T_i]} = \sum_e \rho_e^{[T_i]} v_e, \quad i = 1, \dots, N \quad (2.23)$$

here v_e is the area or the volume of the element. Since in this study, a uniform finite element discretization is used, v_e is constant for all elements.

In the incremental additive manufacturing process, it is crucial that material is deposited onto previously deposited material. Isolated structural fragments require temporary auxiliary structures to hold them in place. To avoid the cost of additional supports, we introduce a continuity constraint that prevents isolated material patches. Such patches correspond to local minima in the time field, with their adjacent elements having larger time values, indicating later fabrication. Hence, isolated material patches are prevented by having

$$g(t_e) = \min_{i \in N_e} (t_i) - t_e \leq 0, \quad \forall e \in M \quad (2.24)$$

wherein N_e denotes the set of elements adjacent to element e . M is the set of active elements in the design domain, i.e., all elements except those which are prescribed as the starting point/region for the fabrication process (i.e., with $t_e = 0$).

Equation 2.24 is non differentiable and has to be approximated by a continuous function. Since $t \leq 1$, $\min_{i \in N_e} (t_i)$ is written as:

$$\min_{i \in N_e} (t_i) = 1 - \max_{i \in N_e} (1 - t_i) \quad (2.25)$$

where $\max_{i \in N_e} (1 - t_i)$ can be approximated with a p-norm [33],

$$\max_{i \in N_e} (1 - t_i) \approx (\sum_{i \in N_e} (1 - t_i)^p)^{\frac{1}{p}} \quad (2.26)$$

Hence $g(t_e)$ can be approximated as,

$$g(t_e) \approx 1 - (\sum_{i \in N_e} (1 - t_i)^p)^{\frac{1}{p}} - t_e \quad (2.27)$$

2.2.4. Space-time problem formulation

Upon introduction of the objective function and the various constraints as discussed above, the formulation for the space-time topology optimization for self weight for intermediate structures stands like:

$$\min : c(x) = U^T K(\rho) U + \sum_{i=1}^N \alpha_i (U^{T_i})^T K(\rho^{T_i}) (U^{T_i}) \quad (2.28)$$

subject to:

$$\begin{aligned}
(K(\rho))U &= F, \\
(K(\rho^{T_i}))(U^{T_i}) &= G(\rho^{T_i}), i = 1, 2, \dots, N, \\
\Sigma_e \rho_e v_e &\leq V_0, \\
0 &\leq \phi_e \leq 1 \\
0 &\leq \tau_e \leq 1 \\
V^{[T_i]} &= \Sigma_e \rho_e^{[T_i]} v_e \leq \frac{i}{N} V_0, i = 1, 2, \dots, N, \\
\frac{1}{(\#M)} \Sigma_{e \in M} H(g(t_e)) &< \epsilon,
\end{aligned}$$

In these equations, c is the compliance, $K(\rho^{T_i})$, U^{T_i} and $G(\rho^{T_i})$ are the stiffness matrix, displacement vector and the force vector for the intermediate structures respectively, K is the fine mesh global stiffness matrix, ϕ_e is the element densities, τ_e is the time field variable for each element, N is the number of elements used to discretize the design domain, v and V are the material volume and design domain volume, and V_0 is the material volume.

2.3. Computational complexity of topology optimization

In the realm of topology optimization using the SIMP (Solid Isotropic Material with Penalization) method, various computational steps contribute to the overall complexity of the process. During each iteration, the assembly of the stiffness matrix, a pivotal step, incurs a complexity of $O(n)$, where 'n' represents the number of degrees of freedom in the mesh. Subsequently, solving the linear Finite Element Method (FEM) equation becomes the most computationally intensive part, with a complexity of $O(n^3)$. This step involves significant matrix manipulations and is directly proportional to the cube of the number of degrees of freedoms.

While the FEM equation solving exhibits the highest complexity, other steps like assembling the stiffness matrix, computing the objective function and sensitivities, and OC-based or MMA-based design updates also contribute to the computational workload of TO. It's important to note that the complexities outlined here serve as general guidelines, subject to variation based on factors like mesh size, problem complexity, and algorithmic implementations.

Evidently, a pivotal strategy for enhancing computational efficiency revolves around diminishing the number of elements and consequently degrees of freedom, primarily affecting the most demanding computational task, the FEM equation solving. The ensuing sections delve into an exploration of diverse coarsening strategies documented in the existing literature.

2.4. Comparison of various coarsening methods

2.4.1. Higher-order multi-resolution topology optimization using finite cell method

The voxel-based variant of the Finite Cell Method (FCM) researched by Duster et al.[16], Parvizian et al.[24], Schillinger[26], employs discrete meshes to delineate both the geometry and the analysis processes. Cells represent the elements engaged in the analysis mesh, while the topology is characterized by density elements known as voxels, which essentially function as volume pixels explained by Groen et al.[18]. This approach allows for a detailed representation of both geometric features and analytical aspects within the FCM framework. A representation of the cell discretization is shown in figure 2.3.

The arrangement of voxels within an individual cell is describable through the parameterization of voxel quantity along a cell direction (n_{voxel}). As such, the overall voxel count in a cell (n_{sc}) becomes reliant on both n_{voxel} and the dimension of the design domain, explained by Groen et al[18]. This parameterization approach offers a versatile means to define the voxel distribution within cells, contributing to the flexibility and adaptability of the method.

For cells featuring intricate material distributions, linear shape functions are inadequate for accurately interpolating the displacement field. As a result, the finite cell method (FCM) incorporates the p-version of the finite element method (FEM). This enhancement allows for improved accuracy in representing complex displacement fields within cells. The utilization of the p-version FEM enhances the FCM's capability to handle varying degrees of complexity in material distributions, making it a robust approach for topology optimization tasks that involve intricate geometries.

The voxel contributions to the cell stiffness matrix (k_c) are incorporated through a composite integration approach. This involves integrating the stiffness matrix and load vector within the voxels, which are then projected onto the cells. The voxel stiffness is interpolated using the solid isotropic material with penalization (SIMP) technique.

$$k_c = \sum_{i=1}^{n_{sc}} (E_{min} + \bar{\rho}_i^q (E - E_{min})) k_i^0 \quad (2.29)$$

where $\bar{\rho}_i$ is the physical density associated with the i^{th} voxel, q is the penalization factor, E is the Young's modulus of a solid voxel, E_{min} is a very small value to avoid ill-conditioning of the stiffness matrix, and k_i^0 corresponds to the contribution of the i^{th} voxel using a unit stiffness.

Integrated Legendre polynomials serve as the foundation for higher-order basis functions. In contrast to Lagrange polynomials, Legendre polynomials possess a hierarchical property, meaning that shape functions for polynomial degree p are included when degree $p + 1$ is utilized.

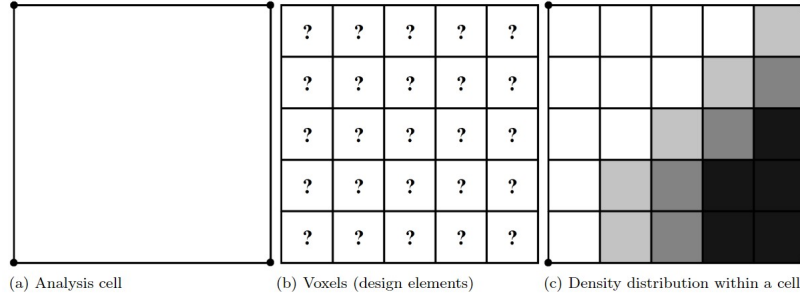


Figure 2.3: Different meshes used in the Finite cell method with $n_{voxel} = 5[18]$

The corresponding one dimensional set of shape functions can be defined as:

$$\begin{aligned} N_1(\xi) &= \frac{1}{2}(1 - \xi) \\ N_2(\xi) &= \frac{1}{2}(1 + \xi) \\ N_i(\xi) &= \phi_{i-1}(\xi), i = 3, 4, \dots, p + 1 \end{aligned} \quad (2.30)$$

where $N_i(\xi)$ corresponds to the i^{th} shape function, and where ϕ corresponds to an integrated Legendre polynomial. With the integrated Legendre polynomials as basis functions, the displacement field can be interpolated:

$$u(\xi) = N_1(\xi)u_1 + N_2(\xi)u_2 + \sum_{i=3}^{p+1} N_i(\xi)u_i \quad (2.31)$$

Here u_1 and u_2 correspond to the nodal displacements, while u_i correspond to the amplitudes of the higher-order shape functions.

Utilizing the p-FEM version to modify the polynomial order of shape functions for specific density elements within this method can lead to heightened computational demands, particularly for higher resolutions featuring intricate and non-homogeneous topologies, explained by Babuka [6]. The expansion in p-degree results in a growing number of nodes, further accentuating the computational complexity, particularly in scenarios of large-scale resolutions.

2.4.2. Design and analysis adaptivity in multi-resolution topology optimization
An MTO element encompasses a finite element (FE), a set of design points, and an overlapping background element equipped with a standardized grid of density cells. All these components share the same spatial domain, a deliberate choice aimed at streamlining integration within an established finite element framework.

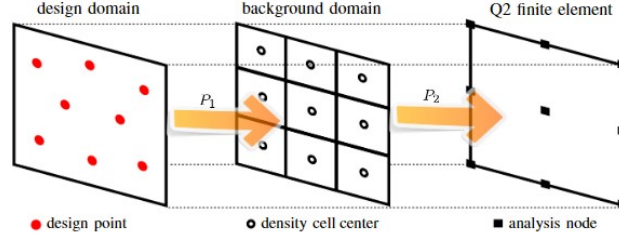


Figure 2.4: Illustrated in this diagram is a Q2/d8 multi-resolution topology optimization element, demonstrating a symbiotic relationship between three interconnected and overlapping domains. On the left, we observe a design domain housing eight strategically positioned design points. In the center, a 3×3 grid of density cells forms a background distribution within the design space. On the right, a Q2 finite element is displayed. Notably, this configuration utilizes projections, labeled as P_1 and P_2 , to seamlessly link the design domain with the background domain and the finite element. The allocation of design points in the domain is accomplished through a modified variant of the k-means clustering approach.[19]

Figure 2.4 illustrates the schematic layout of a Q2/d8 MTO element, utilizing a Q2 finite element characterized by second-order Lagrange quadrilaterals. This MTO element is comprised of eight strategically positioned design points within the domain, arranged non uniformly. The accompanying overlapping background element encompasses a grid of 3×3 density cells. Each of the design points is linked with a density design variable. In the optimization process, these density variables undergo iterative updates driven by the response functions and corresponding design sensitivities.

For achieving adequately uniform arrangements of design points within an element across various numbers of design variables, a modified version of the k-means clustering technique is employed. This method involves partitioning the design domain into approximately equal-sized segments or clusters, denoted as k . The design points are then positioned at the centroids of these identified clusters, thus establishing a balanced distribution.

The attainable resolution limit of the design is influenced by the spacing maintained between the design points. When considering a specific count of design points, a uniform distribution provides the highest achievable resolution without requiring prior knowledge of the optimal design. It's important to highlight that the suggested adaptive MTO method is not restricted to any particular approach for distributing design points; alternative methods for point distribution, such as predefined patterns or other techniques, can also be incorporated as explained by Bruggi et al. [11].

Within the background mesh's density cells, the density is computed employing the P_1 projection method. This calculation exclusively involves design points that reside within the corresponding MTO element. The localized projection serves the purpose of establishing density values for all density cells within the associated MTO element.

Density values at integration points are determined through the projection of densities from the background mesh's density cells. To achieve this, a linear projection method based on density filtering is utilized, following the approach commonly employed in topology optimization. Mathematically, this process can be expressed as follows:

$$\tilde{\rho}_i = \frac{1}{\sum_{j=1}^{n_\rho} H_{ij}} \sum_{j=1}^{n_\rho} H_{ij} \rho_j \quad (2.32)$$

where ρ refers to density values for the cells contained in the background mesh with their centers lying within a distance R from the corresponding integration point, and their number is denoted by n_ρ . Here, terms H_{ij} reduce linearly with distance from the integration point, i.e.,

$$H_{ij} = R - \text{dist}(i, j) \quad (2.33)$$

where $dist()$ denoted the Euclidean distance operator. The background mesh densities are calculated using the P_2 projection from the design mesh to the background mesh. For the p^{th} MTO element, the density of the q^{th} density cell is given as:

$$\tilde{\rho}_q^{(p)} = \frac{1}{\sum_{s=1}^{n_p} h_{qs}} \sum_{j=1}^{n_p} h_{qs} \rho_s \quad (2.34)$$

where ρ_s refers to the density value associated with the s^{th} design point in the design domain contained within the p^{th} MTO element, and lying within a distance r_p from the centroid of its q^{th} density cell. The number of such design points is denoted by n_p , and r_p is the radius of the projection for the p^{th} element. The projection radius r_p needs to be chosen such that it is as small as possible, however, large enough to define densities for all the density cells that correspond to the respective element. It is defined as:

$$r_p = 1.04(dim)^{0.5} \frac{L_p}{d^{1/dim}} \quad (2.35)$$

where dim denotes problem dimension, and L_p is the edge length of the p^{th} MTO element. Note that Equation 2.35 has been obtained empirically through observations based on various design distributions obtained using the k-means clustering approach.

2.4.3. Multi-resolution topology optimization (MTOP)

In this approach, three distinct meshes are employed to address the topology optimization problem effectively. The displacement mesh is utilized for conducting analyses, the design variable mesh is utilized for optimization purposes, and the density mesh is employed to characterize material distribution and calculate stiffness matrices. Design variables represent material densities positioned at the center of density elements. However, it's important to note that the design variable mesh and the density mesh are not necessarily identical. The design variables lack individual physical significance. In the proposed methodology, element densities are derived from design variables through projection functions, allowing for a coherent integration of these mesh-based components.

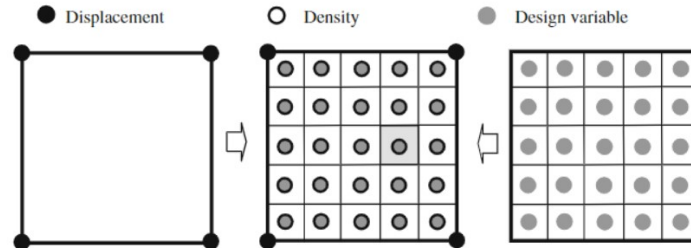


Figure 2.5: The MTOP approach[23]

To achieve a finer level of design resolution, they adopt a density mesh with higher granularity than the displacement mesh, resulting in multiple density elements (sub-elements) within each displacement element. In this arrangement, uniform material density is assumed within each density element. Additionally, a method is introduced to integrate the stiffness matrix, allowing for the incorporation of various density elements within a single displacement element.

In contrast to the adaptive mesh refinement approach, which involves varying the element density based on the presence or absence of material as explained by Sturler[13] and Stainko[29], this method focuses on streamlining computational complexity. Here, element densities are determined via projection functions from design variables. This cohesive integration of mesh-based elements allows for a unified and efficient representation, potentially leading to improved optimization processes with reduced computational overhead.

Within the MTOP framework, the element is labeled as Q4/n25, signifying that each Q4 displacement element encompasses 25 density elements denoted as "n25." The computation of the stiffness matrix involves evaluating the stiffness integrand at 25 integration points, positioned at the centers of the 25 density elements. The associated weight of the integrand corresponds to the area of the respective density element.

The formulation for the stiffness matrix integration is expressed as:

$$K_e = \int_{\Omega_e} B^T D B d\Omega \approx \sum_{i=1}^{N_n} (B^T D B)|_i A_i \quad (2.36)$$

where N_n is the number of integration points in the displacement element domain (N_n is also equal to the number of density elements per displacement element), and A_i is the contribution of density element i to the integration (A_i represents the area/volume of the density element for 2D/3D problems).

From here onwards, this method has been named as the *Trimesh method*. Since the method described by Nguyen is just one among several viable options of multi-resolution strategies, the name *Trimesh method* is used to avoid any confusion.

2.4.4. Coarsening in multigrid methods

Geometric multigrid solvers leverage a hierarchical approach involving progressively coarser grids to address differential equations as explained by Amir et al. [2], Amir et al.[5], Amir et al.[4]. Following several smoothing iterations, a residual is computed at a particular grid level. This residual is subsequently determined for a coarser grid using a restriction operator, explained by Amir et al.[3], Bogomolny[10], Zuo et al.[35], Wang et al.[31]. Utilizing the solution derived from the coarser grid, a correction term is generated and then interpolated to the finer grid. This correction is incorporated into the initial smoothed estimate, thereby yielding the final solution.

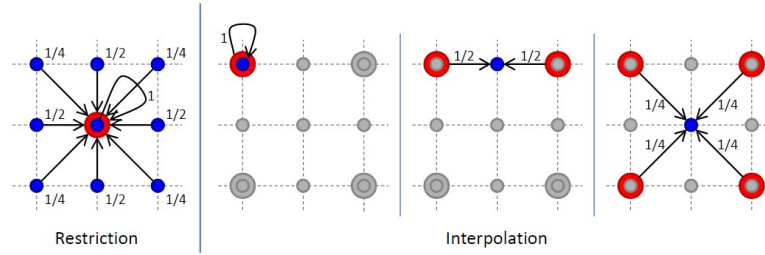


Figure 2.6: Restriction and Interpolation operators[15]

In the context of 2D scenarios, a bilinear operator is employed as an interpolation operator. The corresponding restriction operator, facilitating the transfer of information from a finer mesh to a coarser one, is selected as the transposed form of the interpolation operator. Drawing from Galerkin-based coarsening methods, the system matrix at the coarser level is constructed by combining the restriction operator, the system matrix at the finer level, and the interpolation operator. In a matrix-free approach, the equations at the fine grid vertices are distributed to their coarse grid counterparts for building the coarse grid equation. Subsequently, the fine grid unknowns are interpolated back utilizing the coarse grid unknowns, employing specified weights as depicted in the figure.

In the context that follows, the current level of the grid hierarchy is denoted by a subscript h and the next coarser level by a superscript $2h$, indicating the relative grid spacings between levels. For the multigrid solver, it becomes necessary to have coarse grid versions of the system matrix A along with corresponding restriction and interpolation operators. These operators play a pivotal role in transferring various quantities between consecutive grid levels in the hierarchy.

The multigrid interpolation operator I_{2h}^h is based on bilinear interpolation, while the multigrid restriction operator R_h^{2h} is determined as the transpose of the interpolation operator. Additionally, the approach employs Galerkin-based coarsening, wherein the coarse grid iterations of the system matrix are systematically constructed, progressing from fine to coarse grids. This process ensures a coherent transfer of information across grid levels, facilitating effective multigrid solving strategies.

$$R_h^{2h} = (I_{2h}^h)^T \quad (2.37)$$

$$A^{2h} = R_h^{2h} A^h I_{2h}^h \quad (2.38)$$

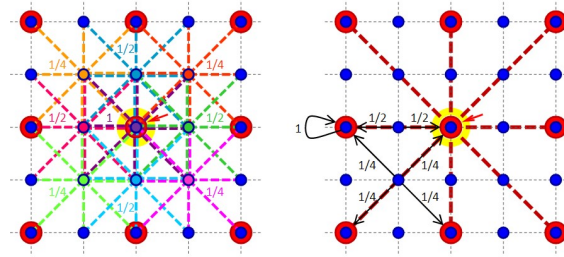


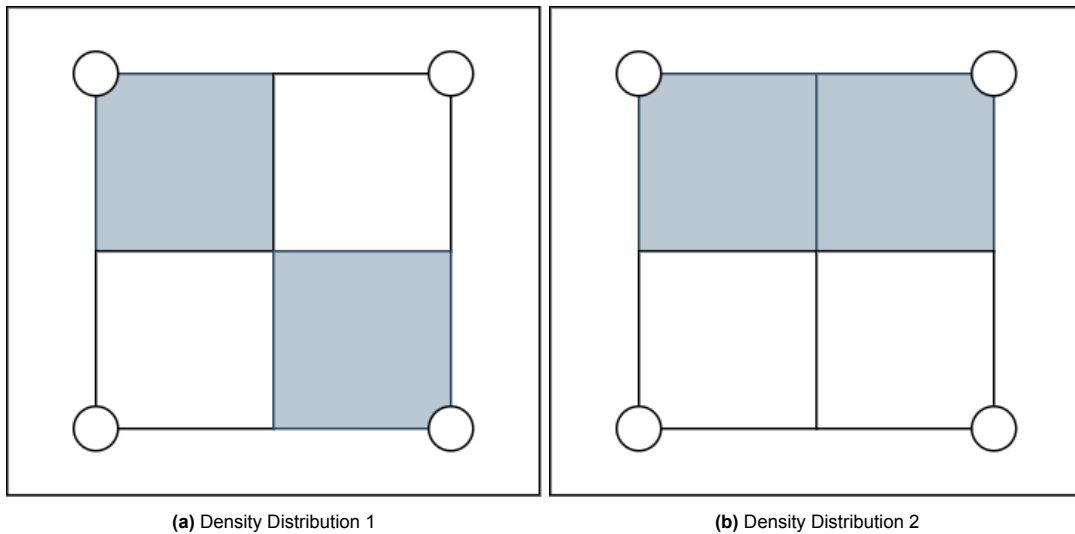
Figure 2.7: Weighted Averaging from fine mesh to coarse mesh[15]

2.4.5. Comparison of coarsening strategies

The dp adaptive method and the method using the Finite cell approach both employ the p-FEM version of solving the finite element equation. p-FEM (polynomial Finite Element Method) is generally more computationally expensive than standard FEM (Finite Element Method). This is because p-FEM involves using higher-order polynomials for shape functions within the elements, which increases the degrees of freedom and consequently the number of unknowns to be solved for. While p-FEM can offer increased accuracy and flexibility in approximating complex solutions, it comes at the cost of increased computational demands, particularly in terms of memory usage and computational time. The higher polynomial order requires more computations for numerical integration, assembling stiffness matrices, and solving linear systems, which can lead to higher computational complexity compared to standard FEM with lower-order shape functions.

In the trimesh method approach, densities within a single displacement cell are aggregated using density penalization, where the weighting factor is determined by the ratio of the area occupied by each fine cell within a coarse cell. This approach eliminates the need for distinct density distributions within a coarse element. While this method is computationally efficient and exhibits rapid convergence, there is a compromise in the accuracy of assembling the stiffness matrix for the displacement cell.

In the context of the multigrid approach, densities within a single displacement cell are aggregated through density penalization, and the weighting factor is determined based on the geometric relationship between coarse mesh nodes and fine mesh nodes. This method offers a distinct contribution from each density value, facilitating the distribution of densities within a coarse element. While this approach involves weighted averaging and isn't as computationally efficient as the trimesh method approach, it provides a more accurate representation of the stiffness matrix as it's developed on a fine mesh, thereby enhancing the accuracy of the optimization process.



(a) Density Distribution 1

(b) Density Distribution 2

Figure 2.8: The stiffness matrix for the assembled 4 densities should ideally capture the difference in distribution of densities.

For instance, when creating a coarsened density representation from a 2×2 fine mesh density set, as illustrated in figure 2.8a and 2.8b, the trimesh method approach fails to distinguish between the depicted density representations. This limitation arises because the trimesh method strategy assigns the same weight to each fine mesh entity, as they all have the same area. In contrast, the multigrid approach, employing weighted averaging, provides a more accurate reflection of density variations. This improved accuracy is achieved by applying appropriate weights to each fine mesh degree of freedom, determined by the geometric relationship, resulting in a more faithful representation of density variations.

A comparison study between the trimesh method approach and the Galerkin method used in multigrid methods is discussed in later chapter.

3

Multi-resolution scheme

This chapter addresses the development of the coarsening operator, its validation, the selection of the interpolation operator, its expansion within the multigrid framework, its extension into three dimensions, and the resulting adjustments to the workflow for both topology optimization and space-time topology optimization.

3.1. Weighted average coarsening

Weighted averaging is the aggregation technique used in creating the coarsening operator. In this method, the density values of the fine grid elements are combined to determine the density of the corresponding coarse grid element. Each fine grid element contributes to the coarse grid element proportionally based on a set of weights. The weights typically depend on the geometric relationship between the fine and coarse grid nodes.

3.1.1. Creating one coarse element

Let's consider a simple example to demonstrate how weighted averaging works. Considering a fine grid of four elements arranged in a 2x2 pattern. Each fine element has its own material density value $(\rho_1, \rho_2, \rho_3, \rho_4)$. The first step towards this would be to assemble the stiffness matrix for this set. Assuming a 2D Q4 element is being used and there are 2 degrees of freedom per node, the assembled global stiffness matrix, K_f would have a size of 18x18. The Galerkin based coarsening method is defined by the formula,

$$K_c = RK_fI \quad (3.1)$$

wherein K_c is the coarse element stiffness matrix, R is the restriction operator and I is the interpolation operator. The restriction and interpolation operator are linked to each other by the following formula,

$$I = R^T \quad (3.2)$$

The restriction operator R is made based on the geometric relationship of the fine grid nodes and the coarse grid nodes as shown in the image. In the Fig 3.1, the red nodes are the overlap between the the fine mesh nodes and the coarse mesh nodes. The blue nodes signify the fine mesh nodes. The weights of each fine mesh node to be interpolated to the coarse mesh node is shown in the image.

Once the coarsened element is created, the coarsened stiffness matrix can be assembled using the coarsened elements to give the coarse mesh stiffness matrix.

3.1.2. Creating the restriction operator for an assembled fine mesh stiffness matrix

In the context of creating the coarse mesh stiffness matrix, there are two distinct approaches to be considered. The first approach involves constructing each coarse element independently from a set of 2x2 fine elements, followed by the assembly of all the individual coarse elements. The second

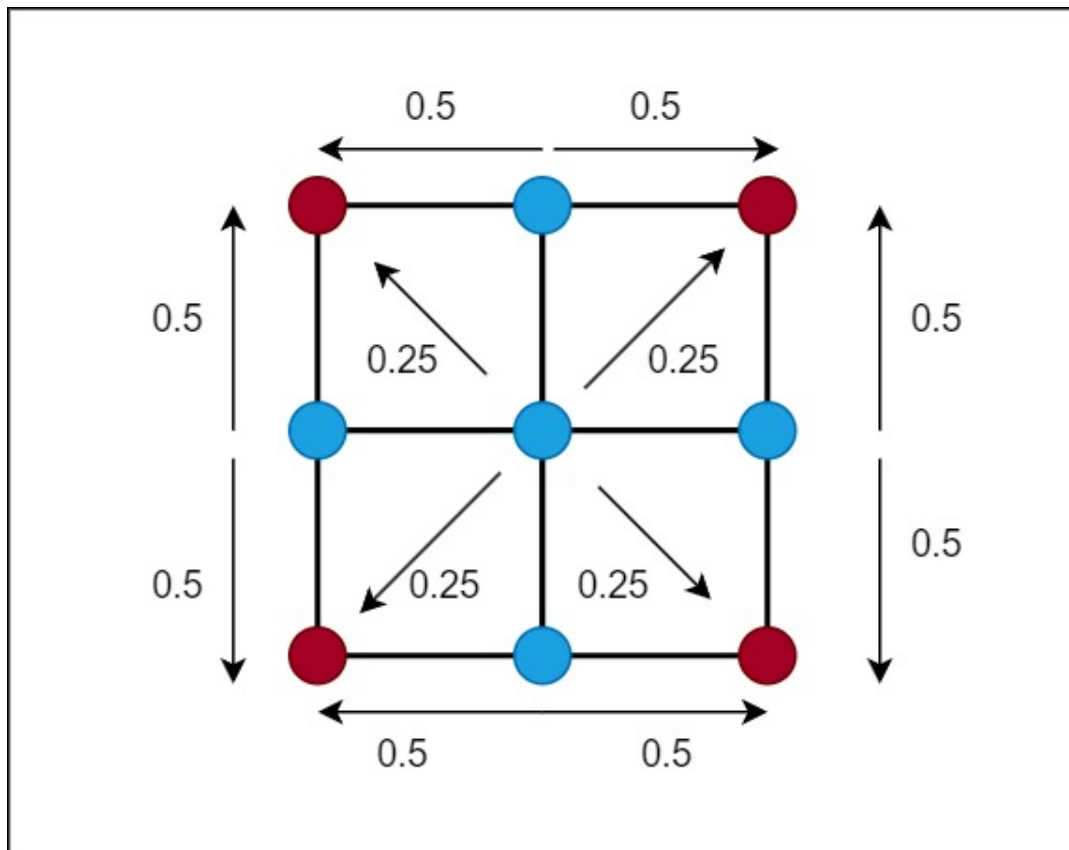


Figure 3.1: Weighted averaging used for creating restriction operator (Red nodes signify overlapping fine and coarse mesh nodes, blue nodes show fine mesh nodes)

approach, on the other hand, entails directly deriving the assembled coarse mesh matrix from the assembled fine mesh matrix using pre-established restriction and interpolation operators tailored for the fine mesh stiffness matrix.

The first approach relies on the discrete representation of the problem, where the fine mesh is initially partitioned into 2×2 fine elements. Each of those fine elements encapsulates local information such as nodal stiffness values and material properties. Subsequently, the coarsening procedure commences by aggregating the nodal information of the 2×2 fine elements into a single coarse element. This aggregation is accomplished through weighted averaging, where the contributions of individual fine element nodes are combined using appropriate weights based on the geometric relationship between the fine and coarse nodes.

Following the creation of the individual coarse elements, the assembled coarse mesh stiffness matrix is formulated by assembling the stiffness contributions of each coarse element. The assembly process ensures that the contributions from overlapping nodes in adjacent coarse elements are properly accounted for, generating a global stiffness matrix for the entire structure at the coarse level.

In contrast, the second approach bypasses the explicit construction of individual coarse elements. Instead, it leverages the established restriction and interpolation operators developed for the fine mesh stiffness matrix. These operators facilitate the transition between the fine and coarse meshes, enabling the derivation of the coarse mesh stiffness matrix directly from the assembled fine mesh stiffness matrix.

The method of creating the restriction operator is based on the geometric relationship of the fine mesh nodes and the coarse mesh nodes. By going along the fine mesh in 2×2 sections, using the same method of weighted averages explained in the previous section the restriction operator can be created. Since the interpolation operator is the transpose of the restriction operator, as per Galerkin based coarsening, the assembled coarse mesh stiffness matrix can be easily generated.

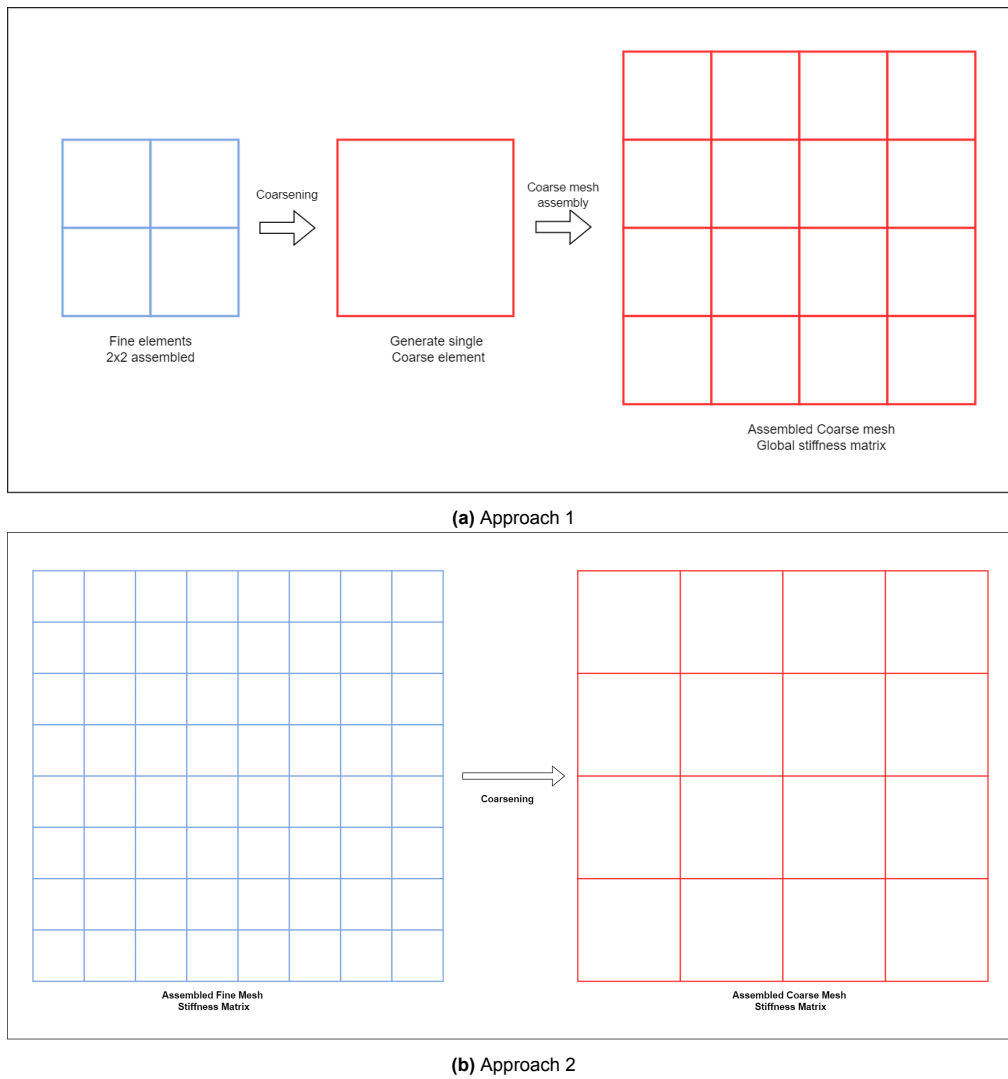


Figure 3.2: Two distinct approaches towards coarsening. Approach 1: Assemble 2x2 fine element set. Perform coarsening to create one coarse element. Assemble coarsened elements. Approach 2: Assemble fine mesh stiffness matrix, perform coarsening to get assembled coarse mesh stiffness matrix

Both approaches serve to achieve a coarsening method for space-time topology optimization, streamlining the computation while preserving the critical structural characteristics.

3.1.3. Comparison of the approaches

The first approach selects 2x2 sections of the fine mesh, assembles the stiffness matrix for the 2x2 section uses the restriction operator for each coarse element and then assembles the coarse mesh stiffness matrix. The second approach creates the restriction operator for the full fine mesh outside the main iteration loop and then uses it on the assembled fine mesh stiffness matrix to create the assembled stiffness matrix for the coarse mesh.

The comparison of computation times for the two approaches are summarised in the following table:

	Assembly time	Coarsening	Solving FEM Equation	Interpolation
One coarse element	50.2		21.7	3.7
Full Restriction operator	28.6	8.9	21.6	3.8

Table 3.1: Comparison of computation times between the full restriction operator and generating single coarse elements. The fine mesh size used was 240x80 elements (All times are in milliseconds)

For a 2D Q4 element, the contribution to a single element k_{ij} in the stiffness matrix from the dimensions for each element is,

$$k_{ij} = \frac{1}{2} \left(\frac{A_2(E^*s_1 + Gs_2) + f_1(E^*s_3 + Gs_4)}{3A_2^2 - f_1^2} + \frac{A_2(E^*t_1 + Gt_2) + f_2(E^*t_3 + Gt_4)}{3A_2^2 - f_2^2} \right) \quad (3.4)$$

where A_2 is twice the area of the element, E^* is either E_1 or E_2 .

$$A_2 = (x_4 - x_2)(y_3 - y_1) - (x_3 - x_1)(y_4 - y_2) \quad (3.5)$$

and

$$f_1 = (x_1 + x_3)(y_4 - y_2) - (x_4 - x_2)(y_1 + y_3) - 2(x_2y_4 - x_4y_2) \quad (3.6)$$

$$f_2 = (x_3 - x_1)(y_4 + y_2) - (x_4 + x_2)(y_3 - y_1) - 2(x_3y_1 - x_1y_3) \quad (3.7)$$

The functions $s_1, s_2, s_3, s_4, t_1, t_2, t_3, t_4$ keep changing for each of k_{ij} . Further knowledge on this can be found in the paper published by Griffith et al. [17].

In summary, understanding the impact of element sizing and appropriately applying scaling factors during coarsening is crucial for maintaining the accuracy and predictive capability of the analysis, while also achieving computational efficiency.

3.3. Validation strategies for the coarsening method

In the pursuit of reliable and accurate multi-resolution space-time topology optimization, the validation of coarsening methods becomes paramount. Two distinct methods of validation are employed in this study to assess the effectiveness and fidelity of the coarsening techniques. The first validation method is a straightforward nature, where a homogeneous density distribution within a 2x2 fine mesh is subjected to coarsening. The aim is to investigate whether the stiffness matrix of the resulting coarsened element, which possesses an identical density distribution, remains unchanged. This fundamental test seeks to confirm whether the coarsening process consistently preserves the stiffness properties when dealing with homogeneous distributions.

In the second validation method, the primary objective is to rigorously assess the accuracy and reliability of the coarsening method employed in the multi-resolution framework. To achieve this, a 2x2 fine mesh with a heterogeneous density distribution is considered, and the coarsening process is applied to generate a new coarse element.

The first step involves utilizing numerical homogenization techniques to determine the macroscopic properties of the heterogeneous material represented by the 2x2 fine mesh. Through this process, the effective material properties of the fine mesh are obtained, enabling the generation of a corresponding coarse element with the homogenized properties as described in figure 3.4.

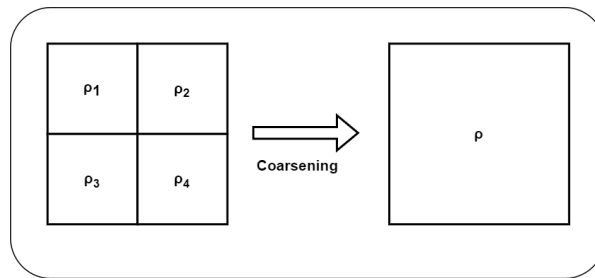


Figure 3.4: Numerical homogenization approach. 4 fine mesh densities are used to generate a single coarsened element

Subsequently, the stiffness matrix of the coarse element derived through numerical homogenization is carefully examined. The objective is to validate whether the coarsening method employed in the multi-resolution space-time topology optimization accurately represents the homogenized stiffness matrix obtained through numerical methods. To facilitate this validation, the stiffness matrix of the coarsened element is compared to the stiffness matrix generated using the coarsening method, specifically the weighted averaging technique. By performing this comparison, the validation confirms the consistency

Density distribution on fine mesh				Match between result from operator and result from homogenization
Density 1	Density 2	Density 3	Density 4	
1	1	1	1	Yes
1	0.5	0.5	1	Yes
0.5	0.75	0.5	0.75	Yes
0.25	0.25	0.25	0.25	Yes

Table 3.2: Range of different fine mesh densities used for validation. The generated coarse stiffness matrix was compared to the coarse stiffness matrix from the operator.

and fidelity of the coarsening process, ensuring that the coarsened element stiffness matrix aligns with the properties through numerical homogenization.

An optimization experiment was executed to compare the performance of the strategy with standard topology optimization. This test utilized identical boundary conditions and mesh resolution for a fair comparison.

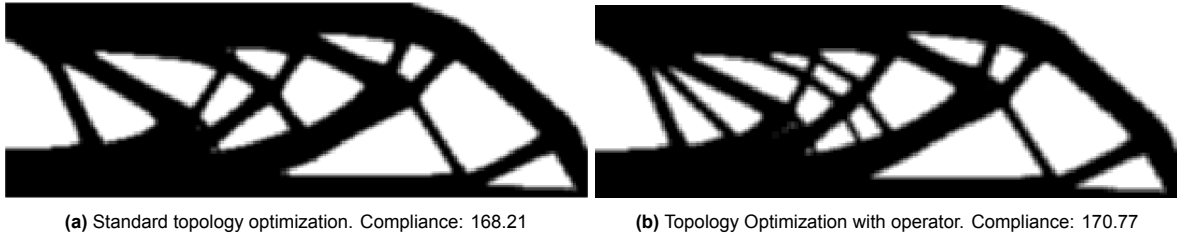


Figure 3.5: Validation of coarsening operator. Compliance values indicate that the coarsening of stiffness matrix has been applied correctly

Through this validation method, the robustness of the coarsening technique is rigorously assessed in handling heterogeneous density distributions and its ability to reproduce the macroscopic properties as shown in figure 3.5. The validation process encompassed the utilization of four distinct density distributions, spanning from entirely homogeneous to significantly heterogeneous density patterns. Subsequently, the stiffness matrix for the coarse element, generated through the trimesh method, was compared against the stiffness matrix derived from the operator, as detailed in table 3.2. The results of this validation serve to build confidence in the coarsening method's accuracy, further reinforcing its sustainability for application in diverse engineering optimization scenarios.

In conclusion, the second validation method primarily focuses on evaluating the coarsening method's performance itself, specifically in capturing the macroscopic properties through numerical homogenization. The aim is to affirm the coarsening method's reliability and consistency, corroborating its efficacy for multi-resolution space-time topology optimization and ensuring the precision of the optimized designs.

3.4. Using the interpolation operator

The choice of the interpolation operator in the context of Galerkin based coarsening holds significant importance in the multi-resolution space-time topology optimization framework. The interpolation operator plays a pivotal role in transferring displacement results obtained from the coarse mesh back to the fine mesh. It ensures consistency and accuracy in the optimization process while preserving fine scale structural details.

Galerkin based coarsening offers a particularly advantageous property in selecting the interpolation operator. It states that the transpose of the restriction operator used for transferring information from the fine mesh to the coarse mesh can be utilized as the interpolation operator for transferring results back to the fine mesh as stated in equation 3.2. This property is known as "coarse-to-fine interpolation", and it simplifies the selection process by exploiting the inherent symmetry between the restriction and interpolation operators.

The interpolation operator serves as the bridge between the coarse and fine meshes, facilitating the

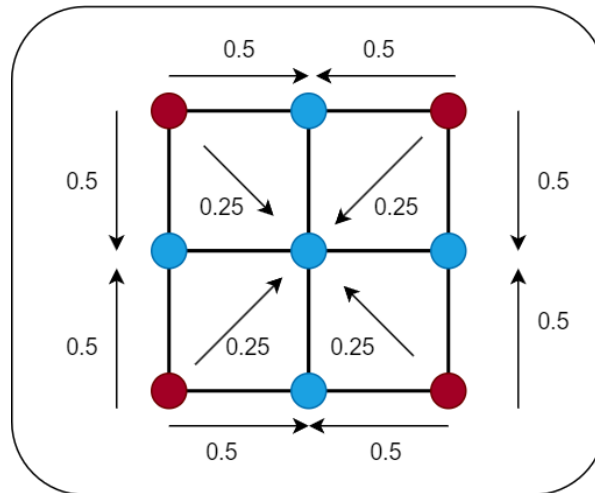


Figure 3.6: Displacement interpolation from coarse mesh to fine mesh (Red nodes signify overlapping fine and coarse mesh nodes, blue nodes show fine mesh nodes)

transfer of computed nodal displacements from the coarse mesh to the corresponding nodes on the fine mesh. The weights used for the interpolation are explained in figure 3.6. They are similar to the weights used in weighted averaging, explained in figure 3.1. By employing the transpose of the restriction operator, the interpolation process ensures that the fine mesh captures the accurate representation of the structural response obtained from the coarse mesh FEM equation solving.

The accurate transfer of displacement results is crucial for maintaining the fidelity of the optimization process. It ensures that the fine mesh, which contains finer scale structural details, appropriately refines the displacement field obtained from the coarse mesh. This refinement is essential for obtaining accurate stress distributions and other fine scale responses, which significantly influence the optimization outcomes.

In summary, the adoption of an interpolation operator plays a crucial role in facilitating a smooth and precise transfer of displacement data from the coarse to the fine mesh within the Galerkin-based coarsening approach. Through harnessing the inherent symmetry between the restriction and interpolation operators, the introduced interpolation method ensures the reliability and integrity of the optimization workflow.

3.5. Extension of the coarsening operator along the lines of multigrid

The coarsening operator has proven to be a valuable tool in enhancing the efficiency of space-time topology optimization by reducing the computational burden associated with large scale engineering problems. In this section, the concept of higher degree of coarsening is explored, where multiple coarsening steps are introduced to generate even coarser versions of the fine mesh stiffness matrix. The changes required in the standard topology optimization workflow to accommodate higher degree of coarsening is discussed and the influence of increased coarsening on the standard density filter is analyzed.

3.5.1. Higher degree coarsening: from 2x2 to 4x4 to 8x8

Higher degree coarsening refers to the successive application of coarsening operators to generate coarser versions of the fine mesh stiffness matrix. Starting with a 2x2 coarsening operator, the process involves applying the coarsening operator once to obtain a 4x4 coarsening, and subsequently applying it twice to obtain an 8x8 coarsening. Each coarser version reduces the number of degrees of freedom further, leading to more significant computational savings. Higher degree coarsening allows for the efficient solution of the FEM equation on successively coarser meshes, making space-time topology optimization even more computationally tractable for large-scale problems.

3.5.2. Incorporating higher degree coarsening in the standard topology optimization workflow

To accommodate higher degree coarsening in the standard topology optimization workflow, certain modifications are necessary. The interpolation of displacements from the fine mesh to the coarser mesh is performed after each coarsening step. Consequently, after solving the FEM equation on the coarsest mesh, the displacements are interpolated back to the finest mesh through a series of interpolation steps. This process ensures that the optimization occurs at the highest resolution while reaping the computational benefits of the coarser mesh during the equation solving step.

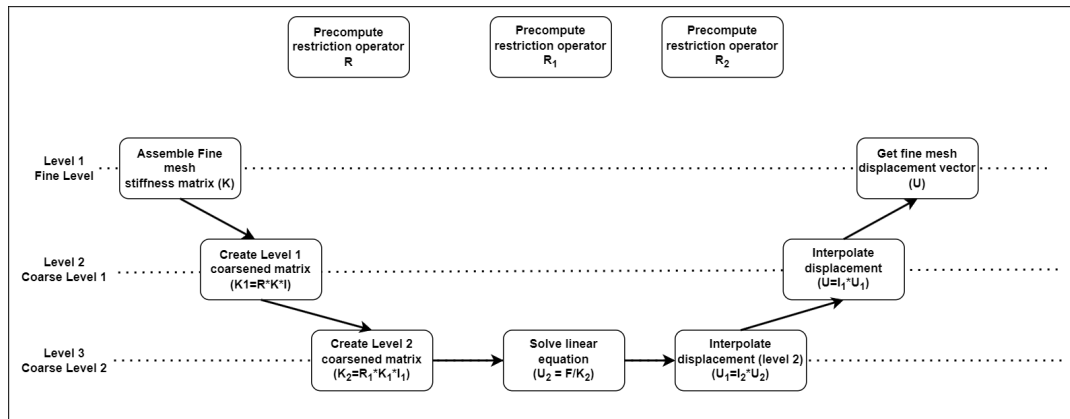


Figure 3.7: Multi level coarsening hierarchy

Both the higher degree of coarsening in topology optimization and the multigrid method (mentioned in section 2.4.4) share certain similarities in their approaches to improve computational efficiency and accelerate convergence. Here are the key similarities between the two techniques:

- **Hierarchy of meshes:** Both methods involve working with a hierarchy of meshes with varying resolutions. In the higher degree coarsening, successive coarsening operators generate coarser versions of the fine mesh stiffness matrix, leading to a hierarchy of coarser meshes. In the multigrid method, a series of nested grids with different levels of resolutions create a hierarchical mesh structure.
- **Coarse mesh solution:** Both techniques aim to solve the problem on coarser meshes to reduce computational burden. In higher degree coarsening, the FEM equation is solved on the coarsest mesh to achieve computational efficiency. In the multigrid method, the problem is solved iteratively on the coarsest mesh as part of the hierarchical correction process.
- **Displacement Interpolation:** Both methods involve the interpolation of results between different mesh levels. In higher degree coarsening, displacements obtained from solving the FEM equation on the coarsest mesh are interpolated back to the finest mesh to ensure the optimization occurs at the highest resolution. In the multigrid method, error information is transferred between different mesh levels and interpolated back to the finest mesh during the error correction process.
- **Convergence improvement:** Both techniques contribute to faster convergence and improved efficiency in solving large-scale engineering problems. The coarser meshes in higher degree coarsening and the error propagation and correction in the multigrid method facilitate better convergence behavior and accelerate the optimization process.
- **Computational savings:** Both methods provide computational advantages by reducing the number of degrees of freedom and the size of the optimization problem. In higher degree coarsening, each coarser version of the mesh reduces the number of elements and degrees of freedom, leading to computational savings. Similarly, the multigrid method leverages the error information to approximate solutions on coarser meshes, reducing the computational effort required for accurate results.
- **Localized smoothing:** Both methods involve some form of localized smoothing to capture fine-scale features and address numerical artifacts. In higher degree coarsening, tuning the density fil-

ter becomes important to achieve accurate and manufacturable designs. In the multigrid method, error propagation and correction are performed iteratively, providing localized corrections to improve the accuracy of the solutions.

In conclusion, the higher degree of coarsening in space-time topology optimization and the multigrid method share several common approaches to enhance computational efficiency and convergence. Both methods utilize a hierarchy of meshes, involve coarser mesh solutions, interpolate results between different mesh levels, and focus on reducing computational burden to achieve faster convergence. By capitalizing on these similarities, engineers and researchers can effectively tackle large-scale engineering problems and optimize designs more efficiently.

To understand the flow of higher order coarsening for a 4x4 case, the flowchart in figure 3.7 has been created.

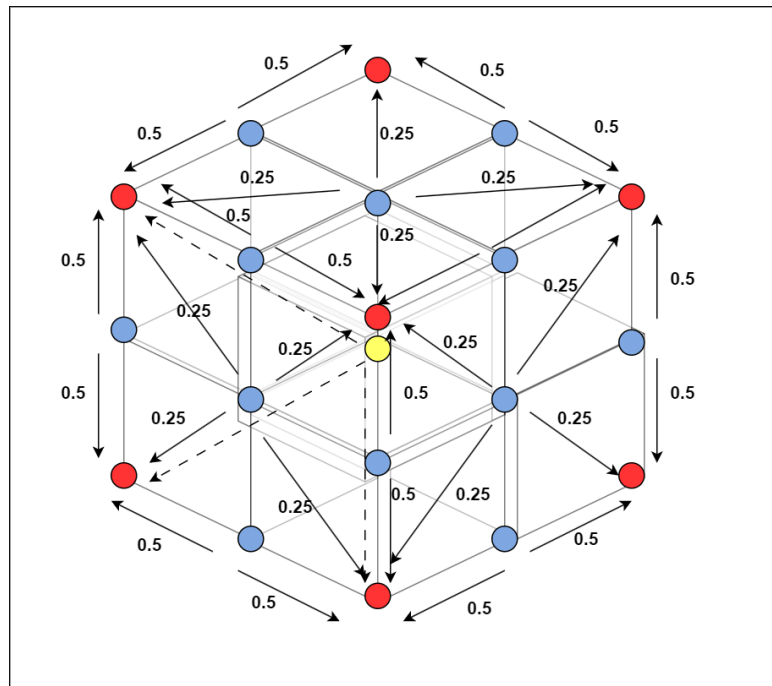


Figure 3.8: Weighted averaging used for the 3D case. The red nodes signify the coarse mesh nodes. The blue nodes signify the fine mesh nodes. The yellow node signifies the fine mesh node shared by the 8 elements of the 2x2x2 mesh. The dotted lines extending from the yellow node to each of the coarse mesh nodes carry a weight of 0.125

3.6. Extension to 3D

In the pursuit of applying the coarsening operator to 3D topology optimization, this chapter delves into the challenges and methodologies involved in defining the restriction operator for coarsening in a three-dimensional environment. The extension to 3D coarsening aims to achieve computational efficiency while preserving fine-scale details and accurately optimizing intermediate structures. Similar to its 2D counterpart, the 3D coarsening operator is based on weighted averaging, the scheme is explained in figure 3.8, leveraging the geometric relationship between fine and coarse mesh elements. Some features of the approach are:

- **FEM solution on coarse mesh:** As in the 2D case, the FEM equation is solved on the coarse mesh during 3D coarsening. By reducing the mesh resolution, the computational effort is significantly decreased, enabling faster FEM equation solving and optimization convergence. The results obtained from the coarse mesh solution are later interpolated back to the fine mesh for compliance calculation.
- **Challenges in restriction operator definition:** One of the primary challenges in the extension to 3D coarsening lies in defining the restriction operator accurately. The restriction operator governs

the transfer of information from the fine mesh to the coarse mesh during coarsening. In 3D, the complexity of element relationships and geometries poses unique challenges in capturing relevant information from the fine mesh and accurately representing it on the coarse mesh.

- **Weighted averaging for restriction:** To address the challenges, the restriction operator is formulated based on weighted averaging, considering the geometric relationship between fine and coarse mesh elements. By carefully assigning weights to the contributions of neighboring fine mesh elements to each coarse mesh element, the restriction operator effectively captures relevant information while maintaining computational efficiency.
- **Preserving fine scale details:** The 3D coarsening operator is designed to preserve fine-scale details during coarsening. The weighted averaging approach ensures that critical design features and material distribution are accurately represented on the coarser mesh levels. This preservation of fine-scale details plays a pivotal role in generating optimal designs that meet performance requirements and manufacturability constraints.

By overcoming the challenges associated with the restriction operator and adopting weighted averaging in a 3D environment, the extension to 3D coarsening enriches the topology optimization process. The chapter sheds light on the methodologies used to adapt the coarsening operator to three-dimensional structures, ultimately contributing to a more efficient and scalable optimization framework for complex engineering problems.

3.7. Topology optimization formulation

3.7.1. Application of operator to topology optimization

The introduction of the operator has a significant impact on several aspects of the optimization process. Specifically, it affects the calculation of the displacement vector U , which plays a crucial role in both the compliance objective function and the constraint represented by the linear equation of finite elements, denoted as $KU = F$. It's important to note that the objective function is computed on the fine mesh, and in this regard, there is no change compared to the formulation of the standard topology optimization problem. This means that the optimization process itself, conducted on the fine mesh, remains consistent with traditional approaches. Furthermore, the sensitivity analysis used to compute the gradients in the optimization process remains unchanged and is akin to the methodology employed in the original topology optimization problem.

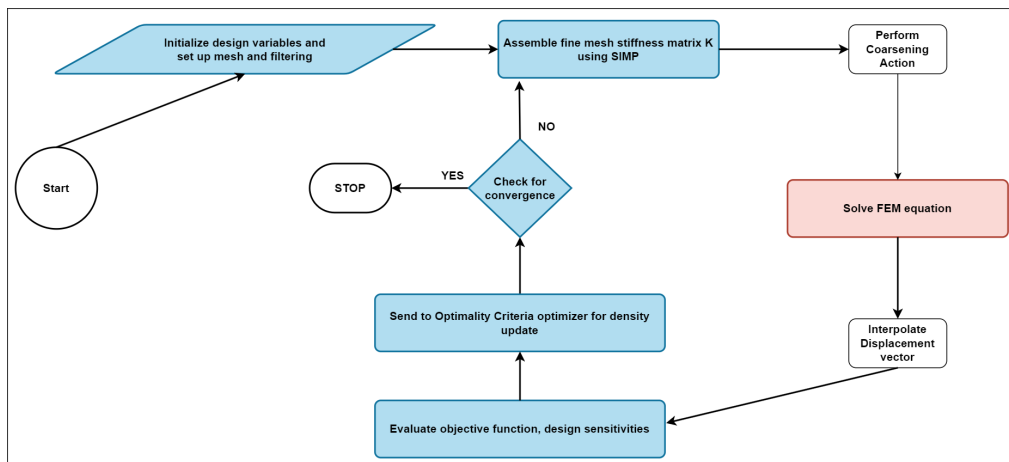


Figure 3.9: The steps for the topology optimization workflow when the coarsening operator is included is explained. Boxes which are marked in blue represent steps carried out on the fine mesh. Boxes which are marked in red represent steps carried out on the coarse mesh.

However, a pivotal alteration occurs when it comes to the linear FEM equation. This equation is calculated on the coarse mesh as explained in figure 3.9, representing one of the key distinctions in the workflow. To bridge the gap between the fine and coarse meshes, an interpolation operator is employed, aligning with the principles of Galerkin-based coarsening. This operator facilitates the transfer of the displacement vector from the fine mesh to the coarse mesh, ensuring that the linear equation

constraint is accurately applied in the coarser representation. This approach allows for a reduction in computational complexity while maintaining the integrity of the optimization process.

3.7.2. Final formulation for topology optimization

On introduction of the restriction operator R and the interpolation operator I , the new formulation becomes:

$$\min : c(x) = U^T K U = \sum_{e=1}^N E_e(x_e) u_e^T k_0 u_e \quad (3.8)$$

subject to:

$$V(x)/V_0 = f \quad (3.9)$$

$$(RKI)U = F \quad (3.10)$$

$$0 \leq x \leq 1 \quad (3.11)$$

In these equations, c is the compliance, U and F are the global displacement and force vectors, respectively, K is the fine mesh global stiffness matrix, u_e is the element displacement vector, k_0 is the element stiffness matrix for an element with unit Young's modulus, x is the vector of design variables (i.e. element densities), N is the number of elements used to discretize the design domain, $V(x)$ and V_0 are the material volume and design domain volume, and f is the prescribed volume fraction. R and I are the restriction and interpolation operators for the coarsening action.

Through this workflow, the proposed optimization process effectively balances computational efficiency and accuracy, capitalizing on the coarse mesh form FEM equation solving while leveraging the fine mesh for detailed optimization and representation of structural behaviour.

3.7.3. Sensitivity analysis for topology optimization

Incorporating the new workflow, subsequent to solving the linear FEM equation within the coarse mesh, the resulting displacement vector is interpolated back to the fine mesh from the coarse mesh. It's on this fine mesh that the objective function and the associated constraints are rigorously evaluated, employing the interpolated displacement vector. Following this comprehensive assessment, the optimizer effectively engages with the density field, facilitating the necessary design updates specifically within the fine mesh domain.

The equation for the sensitivity calculations of the objective for the topology optimization problem are as follows:

$$\frac{\partial c}{\partial x_e} = -p x_e^{p-1} (E_0 - E_{min}) u_e^T k_0 u_e \quad (3.12)$$

The equation for the sensitivity calculations of the volume constraint is as follows:

$$\frac{\partial V}{\partial x_e} = 1 \quad (3.13)$$

In these equations, c is the compliance, U and F are the global displacement and force vectors, respectively, K is the global stiffness matrix, u_e is the element displacement vector, k_0 is the element stiffness matrix for an element with unit Young's modulus, x is the vector of design variables (i.e. element densities), N is the number of elements used to discretize the design domain, $V(x)$ and V_0 are the material volume and design domain volume, and f is the prescribed volume fraction.

3.8. Space-time problem formulation

3.8.1. Application of operator to space-time topology optimization

In the context of space-time topology optimization, the objective function takes on a distinctive structure comprising two integral components. Firstly, the initial part of this function is dedicated to computing the compliance of the entire structural design. Secondly, it delves into calculating the compliance for each intermediate stage or phase of the optimization process. The underlying mathematics of both components involve solving the linear finite element method (FEM) equation, represented as $KU = F$. Notably, for the first part, this equation is solved once, while for the second part, it's solved multiple times, contingent upon the number of predefined stages in the optimization.

With each iteration involving the FEM equation, the coarsening operation is integrated into the standard workflow, resulting in a modification. This process aligns with the depiction illustrated in the figure 3.9. Initially, the stiffness matrix for the fine mesh is assembled. Subsequently, a the coarsening operator is applied to generate an equivalent stiffness matrix for the coarse mesh. This transformation leads to the generation of a displacement vector that needs to be interpolated back into the fine mesh. Post-interpolation, computations ensue on the fine mesh to determine the compliances and their corresponding sensitivities, contributing to the evaluation of the optimization process.

The proposed optimization process effectively balances computational efficiency and accuracy, capitalizing on the coarse mesh form FEM equation solving while leveraging the fine mesh for detailed optimization and representation of structural behaviour. The successful implementation of this workflow demonstrates the practicality and efficacy of the coarsening operator when applied to the space-time topology optimization framework.

3.8.2. Final formulation for space-time topology optimization

Upon introduction of the restriction operator R and interpolation operator I , the formulation for the space-time topology optimization for self weight for intermediate structures stands like:

$$\min : c(x) = U^T K(\rho)U + \sum_{i=1}^N \alpha_i (U^{T_i})^T K(\rho^{T_i})(U^{T_i}) \quad (3.14)$$

subject to:

$$\begin{aligned} (RK(\rho)I)U &= F, \\ (RK(\rho^{T_i})I)(U^{T_i}) &= G(\rho^{T_i}), i = 1, 2, \dots, N, \\ \sum_e \rho_e v_e &\leq V_0, \\ 0 &\leq \phi_e \leq 1 \\ 0 &\leq \tau_e \leq 1 \end{aligned} \quad (3.15)$$

$$\begin{aligned} V^{[T_i]} &= \sum_e \rho_e^{[T_i]} v_e \leq \frac{i}{N} V_0, i = 1, 2, \dots, N, \\ \frac{1}{(M)} \sum_{e \in M} H(g(t_e)) &< \epsilon, \end{aligned}$$

In these equations, c is the compliance, $K(\rho^{T_i})$, U^{T_i} and $G(\rho^{T_i})$ are the stiffness matrix, displacement vector and the force vector for the intermediate structures respectively, K is the fine mesh global stiffness matrix, ϕ_e is the element densities, τ_e is the time field variable for each element, N is the number of elements used to discretize the design domain, v and V are the material volume and design domain volume, and V_0 is the material volume.

3.8.3. Sensitivity analysis for space-time topology optimization

Integrating the novel workflow, following the resolution of the linear finite element method (FEM) equation within the coarse mesh, the resulting displacement vector is subsequently interpolated back to the fine mesh from the coarse mesh. On this fine mesh, evaluation of the objective function and its associated constraints is performed, utilizing the interpolated displacement vector. This comprehensive assessment encompasses compliance evaluations for both the entire structure and intermediate stages. The constraints are applied within the fine mesh framework, followed by the implementation of design updates through the MMA solver.

The sensitivity analysis equations for the volume constraints in equation 3.15 in space-time topology optimization are as follows:

$$\begin{aligned} \frac{\partial V^{[T_i]}}{\partial \phi_e} &= \sum_{k \in S_e} \frac{\partial V^{T_i}}{\partial \rho_k^{T_i}} \frac{\partial \rho_k^{T_i}}{\partial \rho_k} \frac{\partial \rho_k}{\partial \tilde{\phi}_k} \frac{\partial \tilde{\phi}_k}{\partial \phi_e}, \\ &= \sum_{k \in S_e} v_k t_k^{T_i} \frac{\partial \rho_k}{\partial \tilde{\phi}_k} \frac{\partial \tilde{\phi}_k}{\partial \phi_e} \end{aligned} \quad (3.16)$$

where $\frac{\partial \rho_k}{\partial \tilde{\phi}_k}$ follows as:

$$\frac{\partial \rho_k}{\partial \tilde{\phi}_k} = \beta_d \frac{1 - \tanh^2(\beta_d(\eta - \tilde{\phi}_k))}{\tanh(\beta_d \eta) + \tanh(\beta_d(1 - \eta))} \quad (3.17)$$

and $\frac{\partial \tilde{\phi}_k}{\partial \phi_e}$ is calculated based on the definition of $\tilde{\phi}_e$ in equation 2.15.

Similarly, the derivative of constraint regarding τ_e at time T_i is given as:

$$\begin{aligned} \frac{\partial V^{[T_i]}}{\partial \tau_e} &= \sum_{k \in S_e} \frac{\partial V^{T_i}}{\partial \rho_k^{T_i}} \frac{\partial \rho_k^{T_i}}{\partial t_k^{\bar{T}_i}} \frac{\partial t_k^{\bar{T}_i}}{\partial t_k} \frac{\partial t_k}{\partial \tau_e}, \\ &= \sum_{k \in S_e} v_k \rho_k \frac{\partial t_k^{\bar{T}_i}}{\partial t_k} \frac{\partial t_k}{\partial \tau_e} \end{aligned} \quad (3.18)$$

where

$$\frac{\partial t_k^{\bar{T}_i}}{\partial t_k} = \beta_t \frac{\tanh^2(\beta_t(T_i - t_k)) - 1}{\tanh(\beta_t T_i) + \tanh(\beta_t(1 - T_i))} \quad (3.19)$$

and $\frac{\partial t_k}{\partial \tau_e}$ is calculated based on the definition of t_e in equation 2.16.

For the continuity constraint in equation 3.15, the constant $\frac{1}{\#M}$ is dropped out, thus the derivative with respect to time variable τ_e is:

$$\frac{\partial \sum_{e \in M} H(g(t_e))}{\partial \tau_e} = \sum_{i \in S_e} \frac{\partial H(g(t_i))}{\partial \tau_e}, \quad (3.20)$$

where

$$\frac{\partial H(g(t_i))}{\partial \tau_e} = \frac{\partial H(g(t_i))}{\partial g(t_i)} \left(\frac{\partial g(t_i)}{\partial t_i} \frac{\partial t_i}{\partial \tau_e} + \sum_{k \in N_i} \frac{\partial g(t_i)}{\partial t_k} \frac{\partial t_k}{\partial \tau_e} \right), \quad (3.21)$$

with

$$\frac{\partial H(g(t_i))}{\partial g(t_i)} = \beta_m \frac{1 - \tanh^2(\beta_m g(t_i))}{2} \quad (3.22)$$

4

Results and discussion

The boundary conditions shown for the standard topology optimization are shown in figure 4.1.

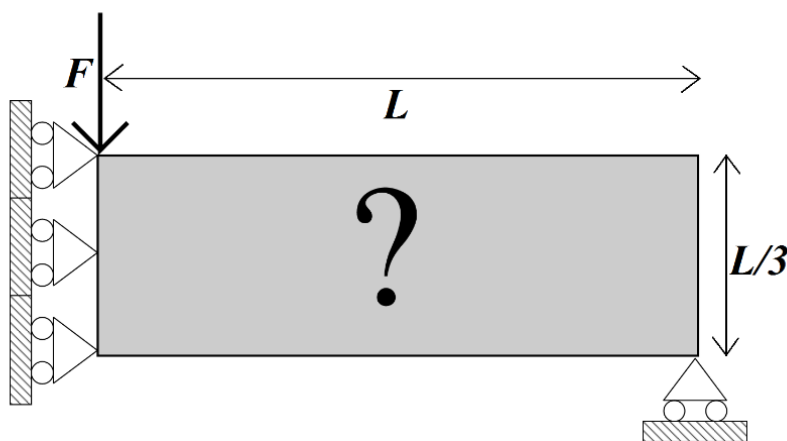


Figure 4.1: Half-MBB Beam Boundary problem [18]

4.1. Topology optimization results with coarsening operator

The coarsening operator was seamlessly integrated into the topology optimization function, with a focus on higher order coarsening using the multigrid approach. The performance of the operator in conjunction with the density filter was examined through a series of tests. While the density filter approach employed the standard density filter, the filter radius required careful calibration to avoid the occurrence of disconnected structures or QR or checkerboard patterns.



Figure 4.2: Disconnected structures arising due to smaller filter radius

For the standard topology optimization, a filter size covering just two elements was adequate. In fig 4.2 it can be seen that structures with such disconnected structures are not manufacturable and hence not practical. Thus a proper choice of filter radius is crucial. The situation changed with higher order coarsening. With 2x2 coarsening, the filter radius had to span at least three elements to maintain design accuracy and prevent numerical artifacts. Similarly, 4x4 coarsening necessitated a filter radius encompassing at least eight fine mesh elements, while 8x8 coarsening demanded a filter radius covering a minimum of 16 fine mesh elements. Striking the right balance between filter radius and coarsening level was critical to achieving successful optimization outcomes.

To test the effectiveness of the coarsening operator and the density filter, standard half MBB beam boundary conditions were utilized. The integration of the coarsening operator, along with appropriately adjusted filter parameters, demonstrated improved computational efficiency and accurate preservation of fine-scale features. The results showcased the potential of the proposed approach to optimize complex structures efficiently while maintaining manufacturability and structural robustness.

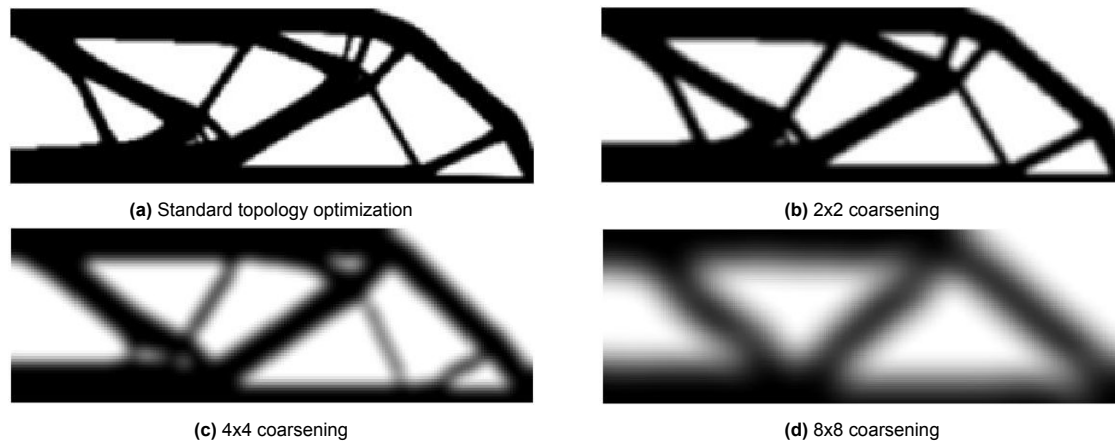


Figure 4.3: Results comparing the geometries for different levels of coarsening

The smoothing effects due to the increase in density filter size gets very pronounced as the the level of coarsening is increased. After 2x2 coarsening, from 4x4 coarsening onwards, fine scale features are lost and thicker structures are produced since the filter radius is very high.

The compliance and computation times for the cases are as follows:

	Assembly	Coarsening	Solving	Interpolation	Compliance	% difference
Standard	30.1	NA	201.25	NA	196.5261	0
2x2	30.4	10.7	64.2	7.9	204.56	4.0879557
4x4	26.2	13.8	13.1	8.5	218.42	11.140454
8x8	32.8	15.9	2.9	10.4	267.34	36.032822

Table 4.1: Table showing the breakup of computation times for assembly of the stiffness matrix, the coarsening operation, solving the FEM equation, Interpolation of displacements, the time taken for the optimizer update, compliance of the final geometry and the percentage difference in compliance with respect to the standard approach(All times in milliseconds)

Observing the results, it becomes evident that as the coarsening degree escalates, there is a noticeable emergence of thicker structures within the design. This phenomenon arises from the necessity to proportionally increase the density filter radius with higher levels of coarsening. This adjustment is crucial to ensure that at least one coarse cell is adequately covered by the filter. As illustrated in figure 4.4, if the filter radius remains set at a lower value, it can lead to discrepancies between material addition, potentially resulting in fragmented or disconnected structural elements.

As the degree of coarsening increases, there is an anticipated rise in compliance values. This increase remains within acceptable limits, hovering around the 5% mark, up to a coarsening factor of 2x2. However, as coarsening becomes more aggressive, there is a notable escalation in compliance.

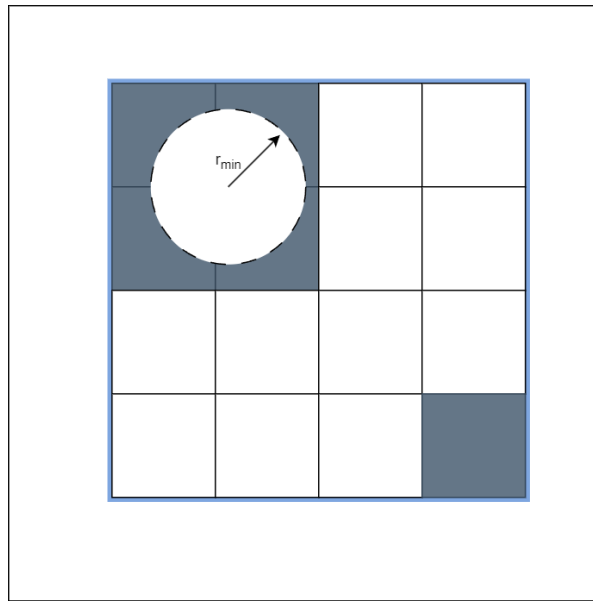


Figure 4.4: The blue outline denotes one coarse element. The grey cells denote elements which are solid. When the filter radius is small, the densities are not properly averaged and hence there might be disconnected densities arising

The tabulated data in table 4.1 underscores another noteworthy trend – a substantial reduction in the time required for solving linear equations. On average, for each successive increase in the degree of coarsening, there’s almost a five fold improvement in computational efficiency.

Nevertheless, it’s essential to highlight that beyond a coarsening factor of 4×4 , the most computationally intensive step shifts from solving the linear equation to the assembly of the fine mesh stiffness matrix. This shift signifies that aggressive coarsening might not be the optimal choice, especially considering the considerable disparity in compliance observed. These findings underscore the delicate balance required between computational efficiency and maintaining structural integrity in the coarsening process

4.2. Space-time topology optimization results

The coarsening operator was successfully integrated into the space-time topology optimization function, enabling higher order coarsening through the multigrid approach. The boundary conditions shown for the space-time topology optimization are shown in figure 4.5. It shows the progress of the robot along the length of the domain. The boundary conditions shown for the space-time topology optimization are

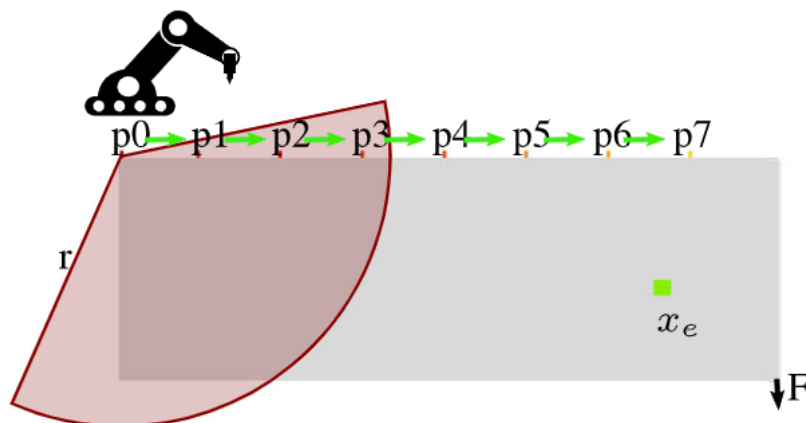


Figure 4.5: A robot printer platform moves along the structure from left to right. The dimensions taken are 3:1 as in the standard half MBB problem [32]

shown in figure 4.5. It shows the progress of the robot along the length of the domain.

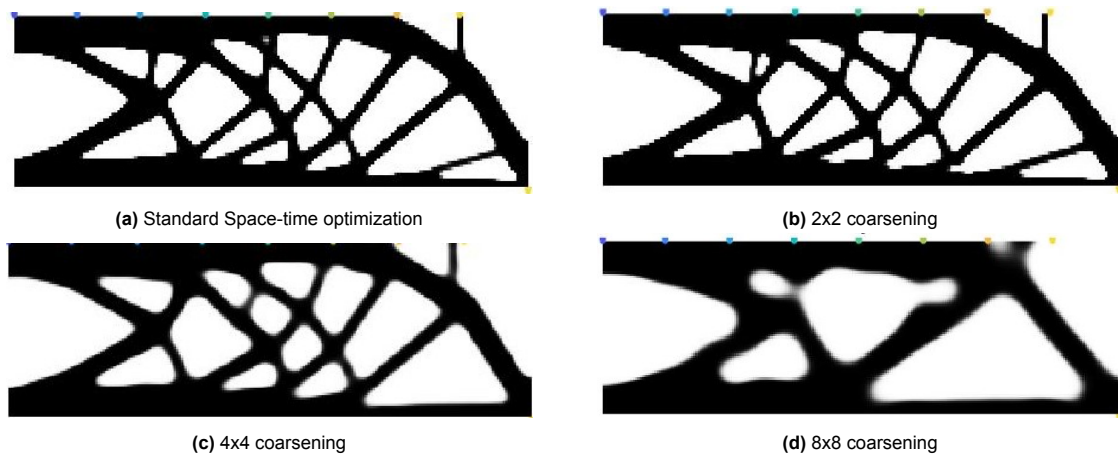


Figure 4.6: Density field after implementing coarsening on space-time topology optimization

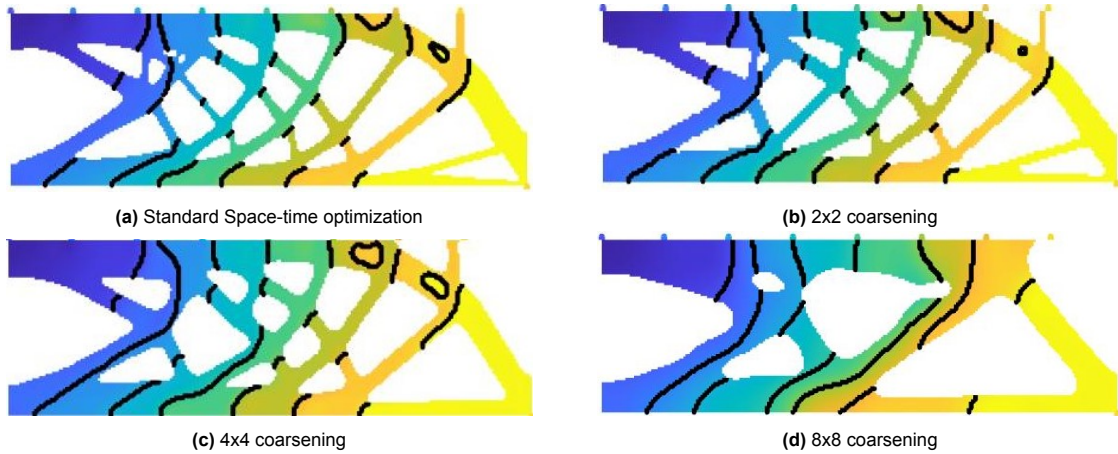


Figure 4.7: Combined Density field and time field (the lines indicate manufacturing order) after implementing coarsening on space-time topology optimization

When applying the density filter with increased filter radii to accommodate higher coarsening levels, the voids in the optimized structures become substantially larger. While the 2x2 coarsening still yields results similar to the standard space-time optimization, the 4x4 coarsening suffers from the effects of a larger filter radius, and the 8x8 coarsening leads to even poorer results. These outcomes highlight the limitations of the density filter in preserving fine-scale features as coarsening levels escalate.

The computation time calculation with regard to the space-time calculation is as shown in table 4.2. As anticipated, the application of higher-order coarsening in standard topology optimization reveals a substantial reduction in the time needed to solve linear equations, even with a slight increase in compliance. However, when extending this approach to space-time optimization, a new complexity emerges. The introduction of the time field, which enables the consideration of multiple intermediate structures, necessitates the solution of additional linear equations in each iteration. Consequently, the decrease in computational time per iteration becomes notably more pronounced in the context of space-time optimization compared to standard topology optimization.

Interestingly, despite this intensified computational burden, the compliance of the final optimized geometry in space-time topology optimization does not exhibit a significant increase. It remains well within the accepted 5% threshold, even up to a coarsening factor of 4x4. This observation highlights the robustness of the proposed coarsening methods, suggesting their applicability in scenarios where computational efficiency is a priority without compromising the structural integrity of the resulting designs.

	Assembly	Coarsening	Solving	Interpolation
Standard - Entire structure	20.4		89.1	
2x2 - Entire structure	18.9	12.6	21.5	7.4
4x4- Entire structure	19.8	14.1	5.4	9.4
8x8- Entire structure	19.9	15.8	0.9	11.2
Standard - Intermediate structure	20		90.1	
2x2 - Intermediate structure	19.2	12.1	20.9	7.4
4x4- Intermediate structure	19.1	14.6	4.1	9.7
8x8- Intermediate structure	19.5	16.1	0.7	10.3

Table 4.2: Computation times for the different coarsening strategies with respect to the entire structure and the intermediate structures are displayed above. The times for the intermediate structure are per stage.

	Assembly	Coarsening	Solving	Interpolation	Compliance	% difference
Standard	180.4	0	809.9	0	231.8468	0
2x2	172.5	109.4	188.7	66.6	233.1257	0.552
4x4	172.6	130.9	38.2	87	235.7426	1.68
8x8	175.9	144.6	6.5	93.6	261.2848	12.7

Table 4.3: Table showing the breakup of computation times for assembly of the stiffness matrix, the coarsening operation, solving the FEM equation, Interpolation of displacements, the time taken for the optimizer update, compliance of the final geometry and the percentage difference in compliance with respect to the standard approach (All times in milliseconds)

As the coarsening level progresses from 4x4 to 8x8, a shift in the dominant contributor to computation time is evident. The assembly of the fine mesh stiffness matrix becomes the primary factor affecting computational efficiency rather than the solving of the FEM equation. Additionally, the extension to 8x8 coarsening leads to a significantly larger difference in compliance values, and the time taken by the optimizer to update the density field experiences a notable increase.

Considering the presented mesh size of 240x80 elements, the results demonstrate the potential challenges and trade-offs associated with incorporating 8x8 coarsening. While increasing the mesh size could potentially alleviate some of the computational demands, this approach was investigated within the current mesh configuration. The findings underline the importance of carefully considering coarsening levels, mesh size, and density filter radius tuning to strike a balance between computational efficiency and design accuracy in topology optimization and space-time topology optimization.

4.3. 3D topology optimization results

The coarsening operator was successfully integrated into the 3D topology optimization function, enabling higher order coarsening through the multigrid approach. The results obtained demonstrate the performance of the operator in conjunction with the density filter. While the density filter approach utilized the standard density filter, careful calibration of the filter radius was required to avoid undesirable QR or checkerboard patterns. For the standard approach, a filter size of 1.2 sufficed, but as coarsening levels increased, larger filter radii became essential. Specifically, for 2x2 coarsening, the filter size needed to cover at least 2 elements, while 4x4 coarsening necessitated a filter radius encompassing at least 4 fine mesh elements. For the most extensive 8x8 coarsening, the filter radius had to span a minimum of 8 fine mesh elements to achieve optimal results. Throughout these tests, half MBB boundary conditions were employed with a mesh size of 96x32x32 elements as illustrated in figure 4.8, providing a consistent benchmark for evaluating the coarsening operator's efficiency and accuracy within the topology optimization framework.

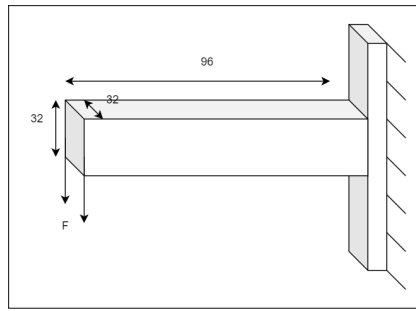


Figure 4.8: Boundary conditions for the 3D simulations

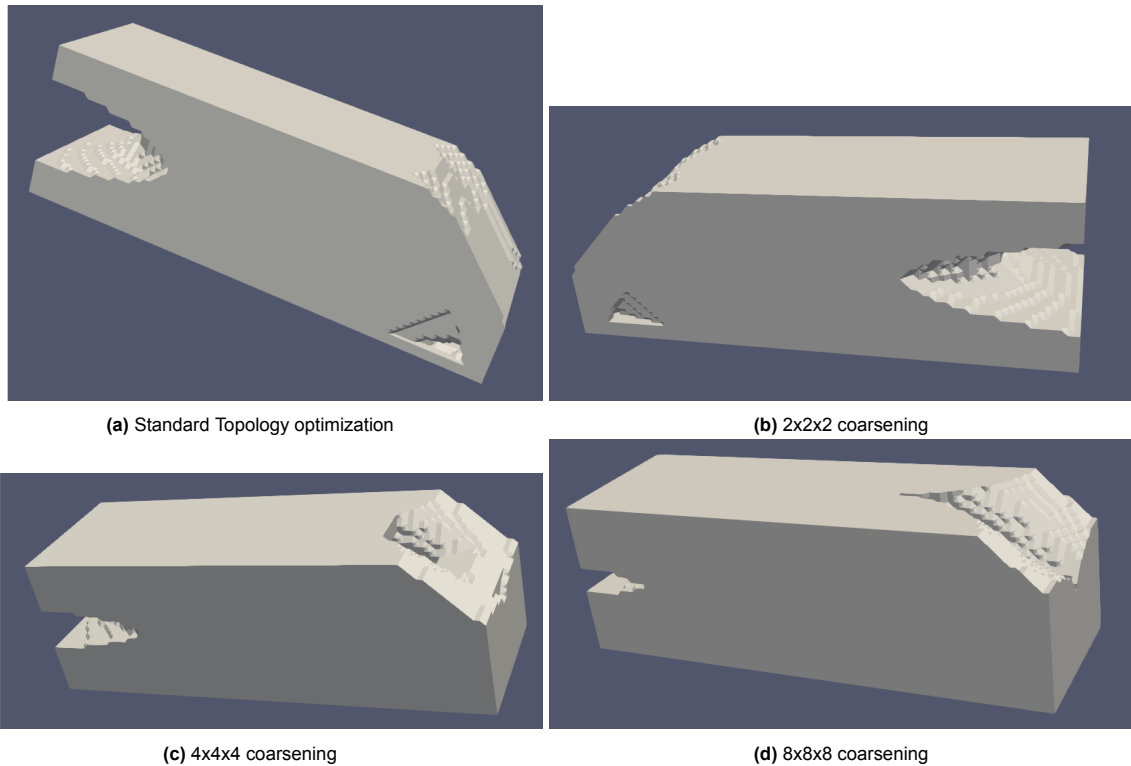


Figure 4.9: Results of higher order coarsening on 3D Optimization

To check for material removal, the structure was sliced along an axis parallel to the Z axis and the results showed that as the level of coarsening is increased, to account for the coarsening, the density filter radius has to be increased. With the size of the density filter being increased, it can be seen in figure 4.10 that the size of the smallest features appearing after optimization keep increasing, which is to be expected.

To compare the computation times and compliances of the generated geometries, refer to table 4.4. The results obtained through 3D optimization align closely with those derived from both standard topol-

	Assembly	Coarsening	Solving	Interpolation	Compliance	% difference
Standard	3417.5	0	338972.4	0	5880.2	0
2x2	3285.9	164.6	11514.2	2.9	6109	3.89
4x4	3518.7	172.4	360.9	3.6	7272.8	23.68
8x8	3330.4	177.3	15.6	4.7	9143.2	55.49

Table 4.4: Table showing the stage by stage computation times and the compliance for each level of coarsening

ogy optimization and space-time topology optimization. Notably, the reduction in time required for

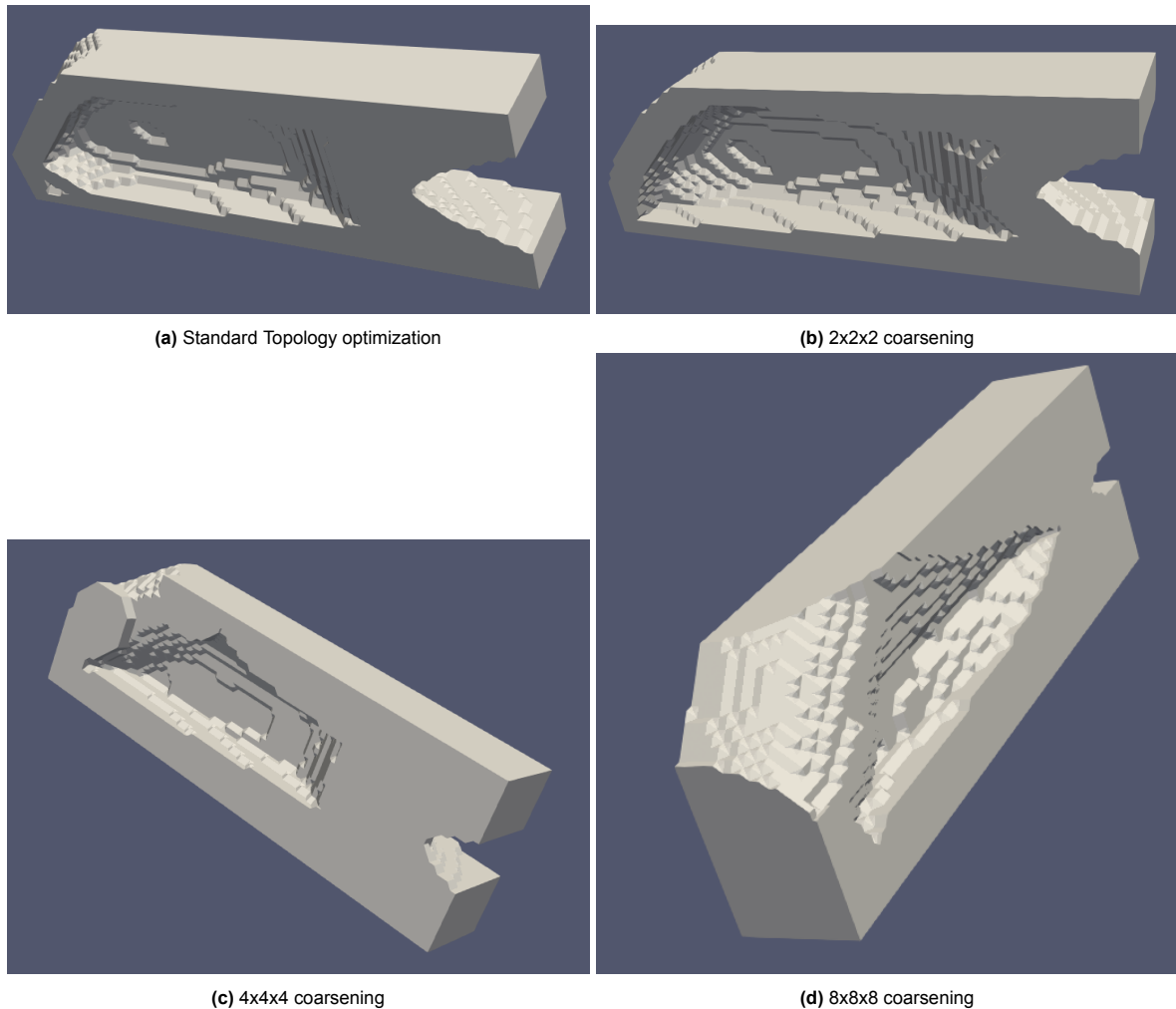


Figure 4.10: Cut slices to show material removal after higher order coarsening on 3D Optimization

solving linear equations in 3D optimization is more pronounced, exhibiting an average decrease of approximately 30 times. This substantial decrease can be attributed to the unique characteristics of 3D optimization. At each stage of coarsening in three dimensions, there is a significantly greater reduction in the number of degrees of freedom that need to be solved for compared to the 2D case. This efficiency gain arises from the inherently higher dimensionality of 3D structures, allowing for a more substantial reduction in computational complexity.

One crucial factor contributing to these results is that the 2D case accounts for the plane stress condition, which does not apply in the 3D scenario. Consequently, the increase in compliance is much more pronounced in 3D optimization, as this aspect is not discounted. Nevertheless, it's important to note that even with the increased compliance, the final optimized designs in 3D remain within the acceptable threshold of 5% for coarsening up to 2x2x2. Beyond this point, there is a significant rise in compliance, which indicates a trade-off between computational efficiency and structural performance that designers must consider when implementing higher-order coarsening in 3D topology optimization.

The selection of the filter radius proves to be a critical aspect in 3D optimizations. As the degree of coarsening intensifies, it becomes imperative to expand the density filter radius to prevent the emergence of disconnected structures. However, this necessary increase in the filter radius has a proportional effect on both the solid structures and voids, leading to a noticeable impact on the final results, as evident in Figure 4.10. Specifically, in the case of 8x8x8 coarsening, the resulting structures exhibit greater thickness compared to those achieved with other coarsening levels. This observation is substantiated by the compliance values illustrated in Table 4.4.

4.4. Comparison with the trimesh method coarsening strategy

Weighted average coarsening stands out for its heightened accuracy in depicting the stiffness matrix. This heightened accuracy stems from its incorporation of weighted contributions sourced from individual density values confined within a single coarse element. This approach ensures that the coarser representation retains a more faithful reflection of the intricate material distribution present at finer scales. By considering the influence of each density value within the larger context of the coarse element, the weighted average coarsening approach manages to provide a superior approximation of the underlying mechanics, making it a preferred choice for scenarios demanding precision and fidelity.

In the trimesh method, a unique approach is employed to aggregate densities within a single displacement cell. This aggregation process relies on density penalization, and the weighting factor is determined by considering the ratio of the area occupied by each fine cell within a coarse cell. A distinct feature of this method is its capacity to eliminate the need for maintaining discrete density distributions within a coarse element. While offering remarkable computational efficiency and rapid convergence, this approach comes with a trade-off in terms of the accuracy of assembling the stiffness matrix for the displacement cell. An illustrative experiment depicted in Figures 2.8a and 2.8b highlights a key limitation of the trimesh method. In this experiment, the areas of each fine mesh element were identical, resulting in equal weights. Consequently, when faced with two separate density distributions, as shown in these figures, the trimesh method struggles to differentiate between them. Consequently, the resulting coarse mesh stiffness matrices would be identical in both cases.

Weighted averaging guarantees that every individual density value makes a proportional contribution to the stiffness matrix of the coarser element. This mechanism results in a more dependable portrayal of the material distribution within the context of the coarser mesh. By upholding this balance between contributions, the weighted averaging approach significantly enhances the accuracy of the overall interpolation process, offering a robust and trustworthy representation of the material's behavior across different scales.

Weighted averaging is particularly advantageous when dealing with finer structures or intricate material distributions that require precise representation. This method excels in capturing the nuances of complex geometries and material arrangements by effectively incorporating the influence of individual density values within each coarser element. This accuracy is crucial for applications where fine-scale details significantly impact the overall performance and behavior of the optimized design.

The computation times comparison for the two approaches are as shown in table 4.5.

The table 4.5 highlights a notable observation: while the trimesh method approach exhibits faster convergence than the Galerkin-based method, the accuracy compromise becomes evident with intensified coarsening in trimesh method. The discrepancy in compliance from the standard approach becomes more pronounced with aggressive coarsening, underscoring a trade-off between speed and accuracy. Conversely, the Galerkin-based weighted averaging approach demands additional time per iteration compared to trimesh method. However, it compensates for this by offering higher accuracy, making it a more reliable and precise strategy in achieving optimal designs.

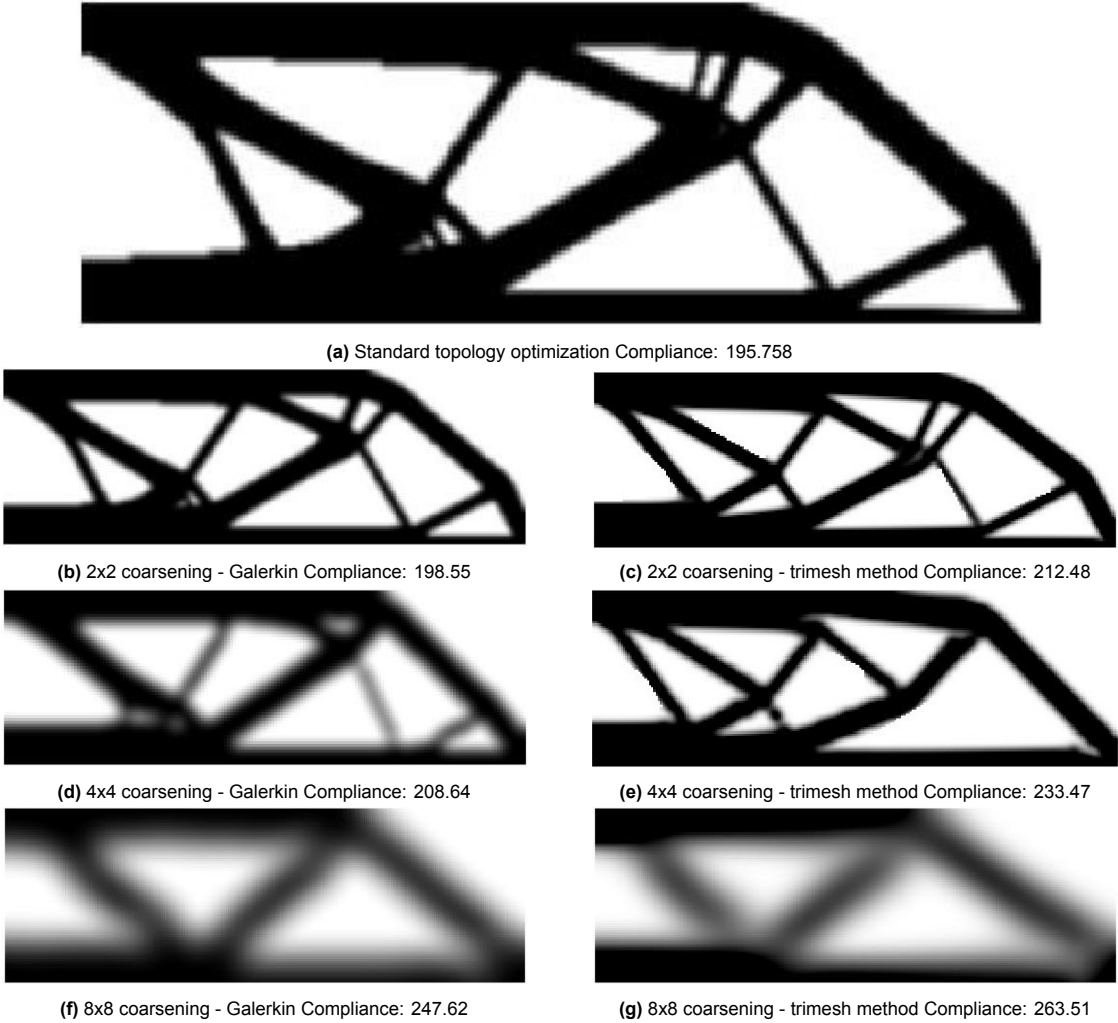


Figure 4.11: Results comparing the geometries for different levels of coarsening

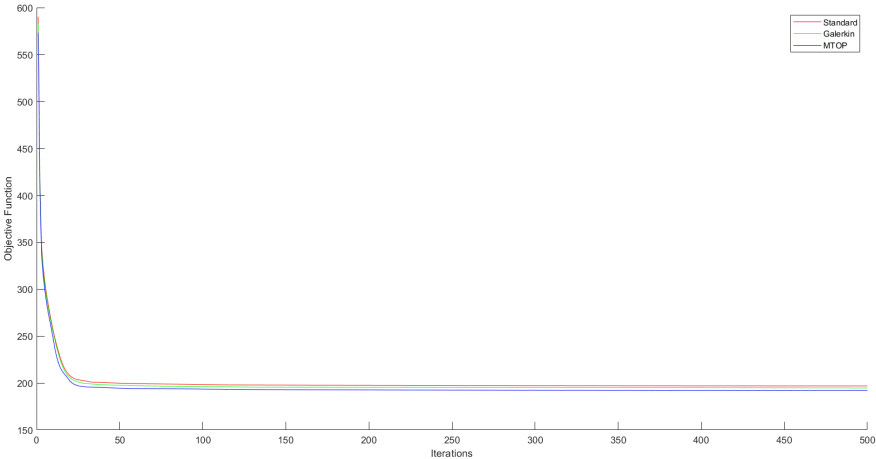


Figure 4.12: Convergence comparison between the standard topology optimization, Galerkin based weighted averaging and the trimesh method approach

	Assembly	Solving	No. of iterations	Total Time	Time per Iteration
Standard	29.4	113.3	739	134152.5	181.53
2x2 (Q4/n4)	19.4	22.2	357	30937.38	86.66
4x4 (Q4/n16)	5.2	4.9	299	17162.9	57.40
8x8 (Q4/n64)	3.4	0.9	139	4766.889	34.29

(a) Comparison of stage wise times for trimesh method approach.(All times in milliseconds)

	Assembly	Coarsening	Solving	Interpolation	Total Time	Steps no.	Time per step
Standard	29.4	0	113.1	0	134152.5	739	181.53
2x2	28.6	8.9	23.7	4.6	83598.47	623	134.19
4x4	29.1	9.1	5.2	4.9	68738.48	796	86.35
8x8	28.7	11.2	0.9	6.1	54694.79	915	59.78

(b) Comparison of stage wise times for the Galerkin based approach. (All times in milliseconds)

	Galerkin		Trimesh method	
	Compliance	% diff	Compliance	% diff
Standard	195.758	0	195.758	0
2x2	198.55	1.43	212.48	8.54
4x4	208.64	6.58	233.47	19.26
8x8	247.62	26.49	263.51	34.61

(c) Comparison of compliance between the trimesh method and the galerkin based methods.

Table 4.5: Comparison of Computation times and compliance values between the trimesh method approach and the Galerkin based weighted averaging approach. (All times in milliseconds)

5

Conclusion and future scope

5.1. Conclusion

In the ever-evolving realm of topology optimization, this thesis embarked on an in-depth exploration of diverse approaches, illuminating their intricacies and implications. The journey began by dissecting traditional techniques like SIMP, revealing their computational complexity, advantages, and challenges.

A pivotal turning point emerged with the introduction of Space-Time Topology Optimization (STTO), a concept that fuses design and fabrication into an integrated whole. By seamlessly incorporating manufacturing order planning into optimization, STTO offers designs that are not only structurally optimal but also inherently manufacturable. This groundbreaking paradigm shift marked a crucial advancement, setting the stage for revolutionary changes in the optimization landscape.

Amid this rich array of methodologies, the Galerkin-based weighted averaging approach shone as a pragmatic balance between computational efficiency and accuracy. While the Multi-Resolution Topology Optimization (trimesh method) approach demonstrated swift convergence, it sometimes sacrificed accuracy under aggressive coarsening. In contrast, the Galerkin approach, with its meticulous attention to preserving the integrity of stiffness matrices, emerged as a more reliable solution for intricate material distributions.

In conclusion, this thesis has navigated through topology optimization's multifaceted landscape, unveiling the diversity and potential of each method. From established techniques to visionary integrations, the journey underscores the intricate balance between computational prowess and precision. As engineering challenges evolve and industries seek lightweight, functional, and sustainable designs, the marriage of computational acumen and creative design thinking becomes paramount. The road ahead lies in the hybridization of methodologies and the continual quest for innovative solutions, shaping the future of optimal design.

5.2. Future scope

While this thesis has provided valuable insights into the coarsening strategies for topology optimization, there are several exciting avenues for further exploration. Some areas that can be looked into in the future are:

- The incorporation of coarsening techniques into the optimization process offers the possibility of optimizing structural designs without the need for displacement interpolation. By evaluating compliance and other desired objective functions directly on the coarse mesh, this modification would streamline the optimization process.
- Further research could be dedicated to investigating the utilization of diverse filtering functions to accommodate coarsening processes and mitigate the emergence of checkerboard patterns. This avenue of exploration aims to enhance the coarsening method's effectiveness by identifying optimal filtering strategies that minimize unwanted artifacts and promote more accurate and reliable

results. Such investigations could contribute to refining coarsening techniques and expanding their applicability in various optimization contexts.

- The trimesh method exhibits accelerated convergence in comparison to the Galerkin-based approach. Future investigations could delve into the underlying factors contributing to this discrepancy, aiming to discern the specific mechanisms or design conditions that lead to the observed differences in convergence rates. This exploration could provide deeper insights into the comparative behaviors of these methods and offer valuable guidance for optimizing their respective strengths in diverse optimization scenarios.

References

- [1] N. Aage and B. S. Lazarov. "Parallel framework for topology optimization using the method of moving asymptotes". In: *Structural and Multidisciplinary Optimization* 47.4 (Apr. 2013), pp. 493–505. DOI: 10.1007/s00158-012-0869-2.
- [2] O. Amir, M. P. Bendsøe, and O. Sigmund. "Approximate reanalysis in topology optimization". In: *International Journal for Numerical Methods in Engineering* 78.12 (June 2009), pp. 1474–1491. DOI: 10.1002/nme.2536.
- [3] O. Amir and O. Sigmund. "On reducing computational effort in topology optimization: How far can we go?" In: *Structural and Multidisciplinary Optimization* 44.1 (July 2011), pp. 25–29. DOI: 10.1007/s00158-010-0586-7.
- [4] O. Amir, O. Sigmund, B. S. Lazarov, and M. Schevenels. "Efficient reanalysis techniques for robust topology optimization". In: *Computer Methods in Applied Mechanics and Engineering* 245-246 (Oct. 2012), pp. 217–231. DOI: 10.1016/j.cma.2012.07.008.
- [5] O. Amir, M. Stolpe, and O. Sigmund. "Efficient use of iterative solvers in nested topology optimization". In: *Structural and Multidisciplinary Optimization* 42.1 (July 2010), pp. 55–72. DOI: 10.1007/s00158-009-0463-4.
- [6] I. Babuka and B. Q. Guo. *The h, p and h-p version of the finite element method; basis theory and applications*. Tech. rep. 1992, p. 174.
- [7] M. P. Bendsoe. *Structural Optimization Optimal shape design as a material distribution problem*. Tech. rep. 1989, pp. 193–202.
- [8] M. P. Bendsøe. *Optimization of structural topology, shape, and material*. Vol. 414. Springer, 1995.
- [9] M. P. Bendsøe and O. Sigmund. *Material interpolation schemes in topology optimization*. Tech. rep.
- [10] M. Bogomolny. "Topology optimization for free vibrations using combined approximations". In: *International Journal for Numerical Methods in Engineering* 82.5 (Apr. 2010), pp. 617–636. DOI: 10.1002/nme.2778.
- [11] M. Bruggi and M. Verani. "A fully adaptive topology optimization algorithm with goal-oriented error control". In: *Computers and Structures* 89.15-16 (Aug. 2011), pp. 1481–1493. DOI: 10.1016/j.compstruc.2011.05.003.
- [12] I. Chivers and J. Sleightholme. "An Introduction to Algorithms and the Big O Notation". In: *Introduction to Programming with Fortran: With Coverage of Fortran 90, 95, 2003, 2008 and 77*. Cham: Springer International Publishing, 2015, pp. 359–364. DOI: 10.1007/978-3-319-17701-4_23. URL: https://doi.org/10.1007/978-3-319-17701-4_23.
- [13] E. De Sturler, G. H. Paulino, and S. Wang. "Topology optimization with adaptive mesh refinement". In: *Proceedings of the 6th International Conference on Computation of Shell and Spatial Structures IASS-IACM*. 2008, pp. 28–31.
- [14] A. Diaz. *Checkerboard patterns in layout optimization*. Tech. rep. 1995, pp. 40–45.
- [15] C. Dick, J. Georgii, and R. Westermann. "A real-time multigrid finite hexahedra method for elasticity simulation using CUDA". In: *Simulation Modelling Practice and Theory* 19.2 (Feb. 2011), pp. 801–816. DOI: 10.1016/j.simpat.2010.11.005.
- [16] A. Düster, J. Parvzian, Z. Yang, and E. Rank. "The finite cell method for three-dimensional problems of solid mechanics". In: *Computer Methods in Applied Mechanics and Engineering* 197.45-48 (Aug. 2008), pp. 3768–3782. DOI: 10.1016/j.cma.2008.02.036.
- [17] D. Griffiths. "Stiffness matrix of the four-node quadrilateral element in closed form". In: *International Journal for Numerical Methods in Engineering* 37.6 (1994), pp. 1027–1038.
- [18] J. P. Groen, M. Langelaar, O. Sigmund, and M. Ruess. "Higher-order multi-resolution topology optimization using the finite cell method". In: *International Journal for Numerical Methods in Engineering* 110.10 (June 2017), pp. 903–920. DOI: 10.1002/nme.5432.

- [19] D. K. Gupta, F. van Keulen, and M. Langelaar. “Design and analysis adaptivity in multiresolution topology optimization”. In: *International Journal for Numerical Methods in Engineering* 121.3 (Feb. 2020), pp. 450–476. DOI: 10.1002/nme.6217.
- [20] HLHRapid. *FDMprinting*. URL: <https://hlhrapid.com/knowledge/what-is-fdm-3d-printing/>.
- [21] C. S. Jog and R. B. Haber. *Computer methods in applied mechanics and engineering Stability of finite element models for distributed-parameter optimization and topology design*. Tech. rep. 1996, pp. 203–226.
- [22] M. Langelaar. “Topology optimization of 3D self-supporting structures for additive manufacturing”. In: *Additive Manufacturing* 12 (Oct. 2016), pp. 60–70. DOI: 10.1016/j.addma.2016.06.010.
- [23] T. H. Nguyen, G. H. Paulino, J. Song, and C. H. Le. “A computational paradigm for multiresolution topology optimization (MTOPT)”. In: *Structural and Multidisciplinary Optimization* 41.4 (Apr. 2010), pp. 525–539. DOI: 10.1007/s00158-009-0443-8.
- [24] J. Parvizian, A. Düster, and E. Rank. “Finite cell method : hh- and p-extension for embedded domain problems in solid mechanics”. In: *Computational Mechanics* 41.1 (2007), pp. 121–133. DOI: 10.1007/s00466-007-0173-y.
- [25] RAMLAB. *RAMLAB/WAAM*. URL: <https://www.ramlab.com/resources/waam-101/>.
- [26] D. Schillinger and M. Ruess. “The Finite Cell Method: A Review in the Context of Higher-Order Structural Analysis of CAD and Image-Based Geometric Models”. In: *Archives of Computational Methods in Engineering* 22.3 (July 2015), pp. 391–455. DOI: 10.1007/s11831-014-9115-y.
- [27] O. Sigmund and J. Petersson. *Numerical instabilities in topology optimization: A survey on procedures dealing with checkerboards, mesh-dependencies and local minima*. Tech. rep. 1998, pp. 68–75.
- [28] O. Sigmund. “On the design of compliant mechanisms using topology optimization”. In: *Journal of Structural Mechanics* 25.4 (1997), pp. 493–524.
- [29] R. Stainko. “An adaptive multilevel approach to the minimal compliance problem in topology optimization”. In: *Communications in Numerical Methods in Engineering* 22.2 (Feb. 2006), pp. 109–118. DOI: 10.1002/cnm.800.
- [30] F. Wang, B. S. Lazarov, and O. Sigmund. “On projection methods, convergence and robust formulations in topology optimization”. In: *Structural and Multidisciplinary Optimization* 43.6 (2011), pp. 767–784. DOI: 10.1007/s00158-010-0602-y.
- [31] S. Wang, E. de Sturler, and G. H. Paulino. “Large-scale topology optimization using preconditioned Krylov subspace methods with recycling”. In: *International Journal for Numerical Methods in Engineering* 69.12 (Mar. 2007), pp. 2441–2468. DOI: 10.1002/nme.1798.
- [32] W. Wang, D. Munro, C. C. Wang, F. van Keulen, and J. Wu. “Space-time topology optimization for additive manufacturing: Concurrent optimization of structural layout and fabrication sequence”. In: *Structural and Multidisciplinary Optimization* 61.1 (Jan. 2020), pp. 1–18. DOI: 10.1007/s00158-019-02420-6.
- [33] J. Wu, C. C. Wang, X. Zhang, and R. Westermann. “Self-supporting rhombic infill structures for additive manufacturing”. In: *CAD Computer Aided Design* 80 (Nov. 2016), pp. 32–42. DOI: 10.1016/j.cad.2016.07.006.
- [34] M. Zhou and G. I. N. Rozvany. *The COC algorithm, Part II: Topological, geometrical and generalized shape optimization*. Tech. rep. 1991, pp. 309–336.
- [35] W. Zuo, T. Xu, H. Zhang, and T. Xu. “Fast structural optimization with frequency constraints by genetic algorithm using adaptive eigenvalue reanalysis methods”. In: *Structural and Multidisciplinary Optimization* 43.6 (June 2011), pp. 799–810. DOI: 10.1007/s00158-010-0610-y.